수의학박사 학위논문

Mechanism of vitamin B_6 effects on hippocampal neurogenesis

비타민B_6가 해마의 신경세포재생에 미치는 영향에 대한 기전 연구

2019 년 8 월

서울대학교 대학원

수의학과 수의해부학 전공

정 효 영

A Dissertation for the Degree of Doctor of Philosophy

Mechanism of vitamin B_6 effects on hippocampal neurogenesis

August 2019

Hyo Young Jung

Suprevisor: Prof. In Koo Hwang, D.V.M., Ph.D.

Department of Veterinary Medicine
Graduate School
Seoul National University

Mechanism of vitamin B_6 effects on hippocampal neurogenesis

지도교수 황 인 구

이 논문을 수의학박사 학위논문으로 제출함
2019 년 4 월

서울대학교 대학원
수의학과 수의해부학 전공
정 효 영

정효영의 수의학박사 학위논문을 인준함
2019 년 7 월

위 원 장 윤 여 성 (인)

부위원장 황 인 구 (인)

위 원 최 정 훈 (인)

위 원 김 대 원 (인)

위 원 유 대 영 (인)

Mechanism of vitamin B_6 effects on hippocampal neurogenesis

Hyo Young Jung, D.V.M.

Supervisor: Prof. In Koo Hwang, D.V.M., Ph.D

Department of Veterinary Medicine

Veterinary Anatomy and Cell Biology

(Major: Veterinary Anatomy)

Graduate School of Seoul National University

Abstract

Vitamin B_6, also known as pyridoxine, acts as a cofactor in more than 160 biochemical reactions. PLP (Pyridoxal 5'-phosphate) is the active form of vitamin B_6 and is involved in the synthesis of several neurotransmitters including serotonin (5-hydroxytryptamine, 5-HT), dopamine (DA), norepinephrine (NE), and GABA. In the central nervous system (CNS), the requirement of pyridoxine is 100-fold more than in the other organs. Vitamin B_6 deficiency affects brain functions by negatively regulating the synthesis of neurotransmitters and may be associated with neurological disorders such as Parkinson disease, depression, etc.

In the present study, we investigated the effects of pyridoxine on hippocampal

functions and changes in protein profiles based on the proteomic approach. Eight-week-old mice received intraperitoneal injections of physiological saline (vehicle) or 350 mg/kg pyridoxine twice a day for 21 days. After, the animals were sacrificed and the brain was dissected out for immunohistochemistry, proteomic analysis, qRT-PCR, and western blot analysis. We found that phosphoglycerate mutase 1 was up-regulated, while CB1 cannabinoid receptor-interacting protein 1 (CRIP1) was down-regulated in the hippocampus of the pyridoxine-treated animals. Additionally, the levels of serotonin and tyrosine hydroxylase were increased in the hippocampus of the pyridoxine-treated group compared to the vehicle-treated group. Furthermore, discrimination indices based on the novel object recognition test were significantly higher in the pyridoxine-treated group than in the vehicle-treated group. Administration of CRIP1a siRNA significantly increased the discrimination index as well as cell proliferation and neuroblast differentiation in the dentate gyrus. In addition, the administration of rimonabant, a CB1 cannabinoid receptor antagonist, for 3 weeks significantly decreased the novel object recognition memory, tyrosine hydroxylase level, cell proliferation, and neuroblast differentiation in the dentate gyrus. Although pyridoxine treatment significantly increased the novel object recognition memory, it slightly ameliorated rimonabant-induced reduction in serotonin, tyrosine hydroxylase level, cell proliferation, and neuroblast differentiation in the dentate gyrus.

In the present study, we also investigated the effects of PGAM1 on novel object recognition, cell proliferation, and neuroblast differentiation in the dentate gyrus. We generated a Tat-PGAM1 fusion protein to cross the blood-brain barrier and neuronal plasma membrane. We administered the Tat peptide, control-PGAM1, or Tat-PGAM1 fusion protein to 8-week-old mice once a day for 3 weeks and tested novel object recognition memory. The mice were then euthanized to conduct western blot analysis for polyhistidine expression and immunohistochemical analysis for Ki67, doublecortin, and

phosphorylated cAMP response element-binding protein. Higher PGAM1 protein expression was observed in the hippocampus of Tat-PGAM1-treated mice when compared with the hippocampi of control, Tat peptide-, and control-PGAM1-treated mice, using western blot analysis. Administration of Tat-PGAM1 and not control-PGAM1 significantly increased the discrimination index as compared to the control group. In addition, the numbers of proliferating cells and differentiated neuroblasts were significantly lower in the Tat peptide-treated group than in the control group. In contrast, the numbers of proliferating cells and differentiated neuroblasts in the dentate gyrus were higher in the Tat-PGAM1-treated group than in the control group. Administration of Tat-PGAM1 significantly facilitated the phosphorylation of cAMP response element-binding protein in the dentate gyrus. Administration of control-PGAM1 did not show any significant effects on novel object recognition, cell proliferation, and neuroblast differentiation in the dentate gyrus.

These results suggest that pyridoxine promotes hippocampal functions by increasing the levels of serotonin and tyrosine hydroxylase immunoreactivity in the hippocampus. This positive effect may be associated with modulating both, CB1 cannabinoid receptor signaling and levels of CRIP1a, and up-regulating the phosphorylation of CREB.

Keywords: vitamin B_6, Hippocampus, Neurogenesis, CB1 cannabinoid receptor-interacting protein 1, phosphoglycerate mutase 1, C57BL/6 mouse

Student Number : 2012-21550

Contents

List of figures

CRIP1a siRNA-treated mice.

Fig 10. Effect of scramble and CRIP1a siRNA on exploration time and discrimination index of familiar vs. novel objects during a novel object recognition test in mice.

Fig 11. Immunohistochemistry for Ki67 and DCX in the dentate gyrus of scramble vs. CRIP1a siRNA-treated mice.

Fig 12. Effect of CB1R inhibition and/or pyridoxine on exploration time and discrimination index of familiar vs. novel objects during a novel object recognition test in mice

Fig 13. Effect of pyridoxine on levels of serotonin (5-hydroxytryptamine, 5-HT), its metabolite (5-hydroxyindoleacetic acid, 5-HIAA), and ratio (5-HIAA/5-HT) in the vehicle-, Pyr-, CB1A-, and Pyr+CB1A-treated groups

Fig 14. Immunohistochemistry for TH, Ki67, and DCX in the dentate gyrus of vehicle-, Pyr-, CB1A-, and Pyr+CB1A-treated groups. Scale bar = 50 μm. The number of Ki67-positive nuclei per section for each group, and the ROD expressed as a percentage of the value of the TH and DCX immunoreactivity in the dentate gyrus of the vehicle-treated group

Fig 15. Purification and identification of control-PGAM1 and Tat-PGAM1 fusion proteins and delivery of these proteins into mouse hippocampus.

Fig 16. Exploration time and discrimination index of familiar vs. novel objects during

testing day of a novel object recognition test in control, Tat peptide-, control-PGAM1-, and Tat-PGAM1-treated mice.

Fig 17. Immunohistochemistry for Ki67 in the dentate gyrus of control, Tat peptide-, control-PGAM1- and Tat-PGAM1-treated mice.

Fig 18. Immunohistochemistry for DCX in the dentate gyrus of control, Tat peptide-, control-PGAM1- and Tat-PGAM1-treated mice.

Fig 19. Immunohistochemistry for pCREB in the dentate gyrus of control, Tat peptide-, control-PGAM1- and Tat-PGAM1-treated mice.

List of abbreviations

2D-DIGE	two dimensional fluorescence difference gel electrophoresis
5-HT	5-hydro-xytryptamine
5-HIAA	5-hydroxyindoleacetic acid
ANOVA	one-way analysis of variance
BBB	blood-brain barrier
CNS	central nervous system
CRIP1a	CB1 cannabinoid receptor-interacting protein 1
CB1R	CB1 cannabinoid receptor
DA	dopamine
DI	discrimination index
DAB	3,3'-diaminobenzidine tetrachloride
DCX	doublecortin
DG	dentate gyrus
DTT	dithiothreitol
F	familiar object
GABA	gamma-aminobutyric acid
GCL	granule cell layer
GLUT3	glucose transporter 3
HIV	human immunodeficiency virus
HPLC	high-performance liquid chromatography
ML	molecular layer
MALDI-TOF MS	matrix assisted lase desorption/ionization time-of-flight mass spectrometry
MAO	monoamine oxidase

N	new object
NE	norepinephrine
PB	phosphate buffer
PBS	phosphate-buffered saline
PCR	polymerase chain reaction
pCREB	phosphorylated-cAMP response element-binding protein
PGAM1	phosphoglycerate mutase 1
PLP	Pyridoxal 5’-phosphate
PoL	polymorphic layer
qRT-PCR	quantitative real time polymerase chain reaction
ROD	relative optical density
SDS	Sodium dodecyl sulphate
SEM	standard error of mean
SGZ	subgranular zone
Tat	Transactivator of transcription
TH	Tyrosine hydroxylase

Introduction

Hippocampus is a major component of the limbic system of the mammalian brain and plays a critical role in learning and memory. It is involved in spatial cognition and storage of long-term memory from short-term memory (Castilla-Ortega et al., 2011; Eichenbaum, 2017; Gould et al., 1999). It comprises of two parts: hippocampus proper (subdivided into CA1, CA2, and CA3) and dentate gyrus(DG). Hippocampus communicates with entorhinal cortex through the trisynaptic circuit. The trisynaptic circuit is a neural circuit, which connect three major regions within the hippocampus: DG, CA3, and CA1. Granule cells in the DG receive projections from the entorhinal cortex via a perforant pathway and synapses on pyramidal cells of CA3 through mossy fibers. CA3 then transmits the signals to pyramidal cells of CA1 via Schaffer collaterals and this projection returns into the entorhinal cortex. DG, CA3, and CA1 in hippocampus make the trisynaptic loop and are integrated into neural circuitry (Deng et al., 2010; Mu and Gage, 2011).

The subgranular zone (SGZ) in the DG of the hippocampus is one of the sites where neurogenesis occurs throughout lifetime. Neurogenesis is the process of generating new neurons from neural stem cells (Goncalves et al., 2016; Gould et al., 1999; Jin, 2016). Previously, it was considered that the adult brain does not regenerate after neuronal cell death. However, since the first discovery of postnatal hippocampal neurogenesis, adult neurogenesis was confirmed by numerous evidence from subsequent studies (Altman and Das, 1965; Deng et al., 2010; Sailor et al., 2016). It has been reported that each day, approximately 9000 new cells are generated in the dentate gyrus and the newly generated granule cells comprise about 6 % of the total granule cell population with the assumption that most of the newborn neurons survive for 4 weeks (Cameron and Mckay, 2001; Prickaerts et al., 2004; Zhao et al., 2008).

New granule cells are generated from neural stem cells in the subgranular zone through successive stages involving proliferation, differentiation, and maturation. Cells at each stage are characterized and distinguished by morphological characteristics. Type 1 cells, also called radial glia-like cell due to their morphology, are the slow cycling, undifferentiated precursor cells in the hippocampus, which gives rise to type 2 cell (intermediate progenitor cells). Finally, type 3 cells (neuroblast) proliferate and exit the cell cycle to differentiate into immature neurons. Maturation of new neurons is characterized by fast axonal and dendritic growth and increased synaptic plasticity. In addition, mature neurons' axon extends to the pyramidal cells of CA3 (Beckervordersandforth et al., 2015; Kempermann et al., 2015). The newly generated and integrated neurons may participate in the neural circuitry function in the hippocampus (Zhao et al., 2008).

Hippocampal neurogenesis is affected in various neurological diseases such as Alzheimer's disease and depression because it is one of the most vulnerable areas of the brain(Mu and Gage, 2011; Sahay and Hen, 2007). In addition, the decrease in neurogenesis with age is closely related to age-related cognitive decline. It has been reported that the hippocampal neurogenesis is regulated by many external stimuli as well as intrinsic factors including physical exercise, learning, stress, hormones, and neurotransmitters. (Balu and Lucki, 2009)

Monoamine neurotransmitters

Monoamine neurotransmitters such as serotonin (5-hydroxytryptamine, 5-HT), dopamine (DA), and norepinephrine (NE) —as well as amino acid neurotransmitters such as γ-aminobutyric acid (GABA) and taurine —are considered as important modulators of mood, emotion, and motor perception and have been implicated in a

variety of other cognitive functions (Feldman and Quenzer, 1984). Several monoamines, including 5-HT and GABA, have been shown to play a role in the regulation of hippocampal neurogenesis (Banasr et al., 2004; Gordon and Goelman, 2016). Monoamines are oxidatively catalyzed by monoamine oxidase (MAO, EC 1.4.3.4) (Edmondson et al., 2004; Tipton et al., 2004), and studies revealed that genetic ablation of MAO A/B in mice increases adult hippocampal neurogenesis as well as synaptic plasticity (Singh et al., 2013). While 5-HT, DA, NE, and GABA are synthesized by their own specific enzymes, they share pyridoxal 5′-phosphate (PLP), an active form of pyridoxine (vitamin B_6), as a major coenzyme.

Pyridoxine, vitamin B_6

Vitamin B_6, also known as pyridoxine, is involved as a cofactor in more than 160 biochemical reactions. PLP is one of the various forms of vitamin B_6 and functions as a coenzyme involved in the synthesis of several neurotransmitters including 5-HT, DA, NE, and GABA (Coburn, 2015; Parra et al., 2018). Pyridoxine is absorbed in the intestine and transported to the liver where it is metabolized to PLP, which is then transported to the muscle, brain, plasma, etc. In the CNS, the requirement of pyridoxine is 100-fold more than in other organs (Spinneker et al., 2007; Yarlagadda and Clayton, 2007). In addition, vitamin B_6 deficiency affects the brain functions by negatively affecting the synthesis of neurotransmitters and may be associated with neurological disorders such as parkinson disease, depression (Malouf and Grimley Evans, 2003). We previously demonstrated that repeated administration of pyridoxine significantly increases cell proliferation and neuroblast differentiation in naïve (Yoo et al., 2011), high-fat diet fed (Yoo et al., 2012b), and D-galactose-induced aging mice (Yoo et al., 2012a).

Although the neurogenic effects of pyridoxine have been reported, the mechanisms

mediating the effects of pyridoxine on hippocampal functions, such as neurogenesis, remain to be elucidated. In the present study, we examined novel object recognition memory and serotonin turnover in the hippocampus. We further investigated the mechanisms of pyridoxine action using two-dimensional fluorescence difference gel electrophoresis (2D-DIGE) followed by matrix-assisted laser desorption/ionization time-of-flight mass spectrometry (MALDI-TOF MS) in mouse hippocampal homogenates, as 2D-DIGE is more sensitive and reproducible than conventional 2D gel electrophoresis (Na et al., 2009; Westermeier and Marouga, 2005; Wilson et al., 2005).

Materials and methods

Experimental design 1

In the experimental design 1, we investigated the effects of pyridoxine on the hippocampus of C57BL/6 mice and conducted proteomic analysis through 2D-DIGE followed by MALDI-TOF MS for studing the mechanism. The experimental animals were divided into two groups: 1) vehicle-treated group, and 2) pyridoxine-treated group.

Experimental Animals

Male C57BL/6J mice (7 weeks of age, n=35) were purchased from Jackson Laboratory Co. Ltd (Bar Harbor, ME, USA). They were housed under standard conditions with feasible temperature (22 ± 2ºC) and humidity (60 ± 5%) control and a 12:12 h light/dark cycle with ad libitum access to food and water. The handling and care of the animals conformed to National Institutes of Health Guidelines for the Care and Use of Laboratory Animals, NIH Publication No. 85-23, 1985, revised 1996). Animal procedures were approved by the Institutional Animal Care and Use Committee (IACUC) of Seoul National University.

Treatment with pyridoxine

The mice were divided into two groups (n = 35 in each group): vehicle (physiological saline)-treated, and 350 mg/kg pyridoxine hydrochloride (Sigma, St. Louis, MO, USA)-treated groups. Vehicle or pyridoxine was intraperitoneally administered to mice at 8 weeks of age, twice a day for three weeks, as described previously (Yoo et al., 2011; Yoo

et al., 2012a; Yoo et al., 2012b).

Novel object recognition test

The testing apparatus consisted of an open box (25 cm × 25 cm × 25 cm) made of black acryl. The floor was covered with woodchip bedding, which was moved around between trials and testing days to prevent the build-up of odour in certain places. The objects to be discriminated were made of solid metal and could not be displaced by the mice due to their weight. The objects were cleaned with bleach to remove residual odours.

On the 20th day of vehicle or pyridoxine treatment (1 h after treatment), mice of each group (n = 20 per group) were allowed to explore the apparatus for 2 min. On the testing day (21st day of treatment), two 2-min trials were performed 1 h following the last treatment. In the “sample” trial (T1), two identical objects were placed in two opposite corners of the apparatus. A mouse was placed in the apparatus and left to explore these two identical objects. After T1, the mouse was placed back in its home cage for an inter-trial interval of 1 h. Subsequently, a “choice” trial (T2) was performed. In T2, a new object (N) replaced one of the objects presented in T1. The mice were exposed again to two different objects: the familiar (F) object and N. Exploration was defined as directing the nose toward the object at a distance of no more than 2 cm and/or touching the object with the nose. From this measure, a series of variables were then calculated: the total time spent in exploring two identical objects in T1, and the time spent in exploring two different objects (F and N) in T2. The distinction between F and N in T2 was determined by comparing the time spent exploring F with that spent exploring N. The dissimilarity index (DI) represents the difference in exploration time expressed as a proportion of the total time spent exploring the two objects in T2.

Tissue processing

Animals (n = 5 per group) were anesthetized with 1 g/kg urethane (Sigma-Aldrich, St. Louis, MO, USA) at 3 weeks after treatment. They were perfused transcardially with 0.1 M phosphate-buffered saline (PBS; pH 7.4), followed by 4% paraformaldehyde in 0.1 M PBS (pH 7.4). The brains were removed and postfixed in the same fixative for 12 hours before undergoing cryoprotection via overnight storage in 30% sucrose. Serial coronal brain sections (30 μm) were generated using a cryostat (Leica, Wetzlar, Germany) and collected into six-well plates containing PBS.

Immunohistochemistry for Ki67 and DCX

To ensure that the histochemical and immunohistochemical data were comparable between groups, sections were carefully processed under parallel conditions. Tissue sections were selected between 1.46 mm and 2.46 mm posterior to the bregma by referring to the mouse atlas by Franklin and Paxinos (Franklin and Paxinos, 1997)
Five sections from tissue sections located 90 μm apart were sequentially incubated with 0.3% hydrogen peroxide (H_2O_2) in PBS for 30 minutes and 10% normal goat serum in 0.05 M PBS for 30 minutes. Sections were then incubated with a rabbit anti-Ki67 antibody (1:1,000; Abcam), rabbit anti-doublecortin (DCX) antibody (1:5,000; Abcam) overnight at room temperature, followed by incubation with biotinylated goat anti-rabbit IgG, and then by a streptavidin-peroxidase complex (1:200, Vector, Burlingame, CA, USA). Immunostaining was visualized by reaction with DAB in 0.1 M Tris-HCl buffer (pH 7.2). Sections were dehydrated and mounted on gelatin-coated slides in Canada balsam (Kanto, Tokyo, Japan).

Estimation of levels of monoamine and its metabolites in the hippocampus

Quantification of serotonin and its metabolite by high-performance liquid chromatography

The concentrations of 5-HT and 5-hydroxyindoleacetic acid (5-HIAA) in hippocampal homogenates were determined using high-performance liquid chromatography (HPLC) as described by Nadaoka et al (Nadaoka et al., 2012). Briefly, an aliquot of processed homogenate was injected onto a C_{18} reverse-phase column (250 mm × 4.6 mm, 5 μm; Agilent Technologies, Santa Clara, CA, USA) in an HPLC system (Agilent 1100 series, Agilent Technologies) equipped with an electrochemical detector. The mobile phase (0.1 M acetate-citrate buffer with 17% methanol) allowed for the separation of 5-HT and its metabolite, 5-HIAA (Rowland and Dunn, 1995). Sodium octyl sulfate (190mg/L) was added as an ion-pairing agent, and EDTA (5mL) was added as a n antioxidant. Each peak area was normalized to isoproterenol concentration. The level of 5-HT, its metabolite were detected by using a Waters 474 scanning fluorescence detector (Waters, Milford, MA, USA). All detected compounds were quantified by comparing the area under the peaks with the area of reference standards by using specific HPLC software (Chromatography Station for Windows). The turnover ratio of 5-HIAA to 5-HT is considered an index of cell activity that results in the release, re-uptake, and metabolism of 5-HT to 5-HIAA.

Examination of tyrosine hydroxylase activity by immunohistochemical staining

To observe the effects of pyridoxine on dopamine levels in the hippocampus, an immunohistochemical study was conducted for tyrosine hydroxylase (TH), the

synthesizing enzyme of dopamine. As previously described, five sections from tissue sections located 90 μm apart were sequentially incubated with 0.3% hydrogen peroxide (H2O2) in PBS for 30 minutes and 10% normal goat serum in 0.05 M PBS for 30 minutes. Sections were then incubated with a rabbit anti-TH antibody (1:1,000; Milipore, Temecula, CA, USA) overnight at room temperature, followed by incubation with biotinylated goat anti-rabbit IgG, and then by a streptavidin-peroxidase complex (1:200, Vector, Burlingame, CA, USA). Immunostaining was visualized by reaction with DAB in 0.1 M Tris-HCl buffer (pH 7.2). Sections were dehydrated and mounted on gelatin-coated slides in Canada balsam (Kanto, Tokyo, Japan).

2DE-DIGE

Protein preparation

The 2D-DIGE procedure was performed under conditions of darkness, as described by Na et al (Na et al., 2009). Vehicle (n = 20)- and pyridoxine (n = 20)-treated animals that had completed the novel object recognition test were anesthetized with 2 g/kg urethane (Sigma-Aldrich), following which hippocampal tissues were isolated from the brain. Hippocampi were suspended in the sample buffer, which consisted of 30 mM Tris, 7 M urea, 2 M thiourea, 65 mM dithiothreitol (DTT), and 4% 3-[(3-cholamidopropyl)dimethylammonio]-1-propanesulfonate [CHAPS]) with 40 μL protease inhibitor (pH 8.5). Suspensions were sonicated five times for 10 s and centrifuged at 45,000 rpm for 45 min. Proteins in the supernatants were quantified using the 2D Quant kit (GE Healthcare, Uppsala, Sweden).

Labelling with CyDye™ and separation of proteins

For CyDye labelling, 1 μL of Cy5 working solution (400 pmol) and 1 μL of Cy3 working solution (400 pmol) were added to two samples of hippocampal homogenates from vehicle- and pyridoxine-treated groups (50 μg). Samples labelled using each CyDye™ DIGE fluor (Cy2, Cy3, and Cy5) and 2× buffer (2 M thiourea, 7 M urea, 2% Pharmalayte®, 130 mM DTT, 4% CHAPS, and trace of bromophenol blue) were used for 2-D DIGE analysis. Mixed samples were loaded into the anode cup of a Multiphor II IEF system (GE Healthcare Bio-Sciences). First dimensional isoelectric focusing started from 100 V for 3 h and gradually increased to a final voltage of 8000 V. A total of 80,000 V/h was provided by setting the maximum current to 75 μA. To make a preparative picking gel for identification of protein spots, 2 mg of preparative hippocampal protein samples were mixed with rehydration buffer (6 M Urea, 2 M thiourea, 4% CHAPS, 0.4% DTT, 2% v/v IPG buffer pH 3 to 10, pH 6 to 11 and pH 4 to 7) to a final volume of 450 μL. For the DIGE experiment, 8% to 16% linear gradient sodium dodecyl sulphate (SDS) polyacrylamide gels were made using low fluorescent glass plates, and a general glass plate (200 mm × 250 mm × 1.0 mm) was applied for the preparative gels. The equilibrated IPG strips after the first dimension electrophoresis were placed onto SDS polyacrylamide gels. The gels were placed into the 24-cm Ettan DALT twelve system (GE Healthcare Bio-Sciences), then run at 2.5 W per gel for 30 min and at 12 W per gel for 7 min.

DIGE gel image detection

After washing each low-fluorescence glass plate with distilled water, fluorescence images were viewed using Typhoon 9410 Variable Mode Imager (GE Healthcare Bio-Sciences) with ImageQuant Software (GE Healthcare Bio-Sciences) and analysed using DeCyder V.5.0 Software (GE Healthcare Bio-Sciences) (Na et al., 2009). The gel images

were analysed gel-to-gel, and matching of the standard spot maps from each gel was performed using the DeCyder biological variation analysis module. This allowed for the statistical analysis of changes in protein abundance between the samples. Paired Student's *t*-tests were performed for each matched spot set. Differences were considered statistically significant at *p*-values less than 0.05. The Coomassie brilliant blue (CBB)-stained gels were analysed using ImageScanner II (GE Healthcare Bio-Sciences) with ImageMaster 2D platinum software version 5.0.

MALDI-TOF MS

Protein spots of interest were isolated from the preparative gel into 1.5 mL Eppendorf tubes, as described in a report by Na et al (Na et al., 2009). Briefly, mass spectra of peptides were obtained using the 4800 MALDI-TOF analyser (Applied Biosystems) in reflection/delayed extraction mode with an accelerating voltage of 20 kV, and the data from 500 laser pulses were summed. The spectrum was calibrated with trypsin auto-digested peaks (m/z: 842.5090 and 2211.1046), and monoisotopic peptide masses were obtained using Data Explorer 4.4 (PerSeptive Biosystems). A mass range of 800-4000 m/z was used with 1000 shots per spectrum. At the end of the macro process, raw data were generated regarding the centroid mass, resolution, height, and S/N ratio of each peak. These data were converted to an Excel file and used for the MASCOT (Matrix Science, London, UK; version 2.2.04) search to identify peptide sequences present in the protein sequence database NCBInr (mouse). Protein scores higher than 67 were regarded as significant ($p < 0.05$).

The protein of interest (up- or down-regulated) was defined from the Cy3 or Cy5 images and matched to its corresponding spot in CBB-stained preparative picking gel images. The protein spots were manually excised, subjected to in-gel digestion, and

analysed using MALDI-TOF MS. Raw spectra of samples were processed using DataExplorer software to remove and reduce the noise, producing a list of monoisotopic peaks. The tryptic peptide masses were used to search for protein candidates using the web-based searching software ProFound (http://129.85.19.192/profound_bin /Web ProFound.exe).

Result validation by western blot and quantitative real-time polymerase chain reaction (qRT-PCR) analysis

For qRT-PCR and western blot analysis, mice (n = 5 in each group) from vehicle- and pyridoxine treated groups were anesthetized with 2 g/kg urethane (Sigma-Aldrich), following which hippocampal tissues were isolated from the brain. Left and right hippocampi were used for qRT-PCR and western blot analysis, respectively.

qRT-PCR analysis

For PCR analysis, mice (n = 5 in each group) from vehicle- and pyridoxine treated groups were anesthetized with 2 g/kg urethane (Sigma-Aldrich), following which hippocampal tissues were isolated from the brain. Left and right hippocampi were used for qRT-PCR and western blot analysis, respectively. RNA extraction was performed using a total RNA isolation kit (Macherney-Nagel). Spectrophotometric measurements were conducted using the Nanodrop Spectrophotometer (Nanodrop Technologies Wilmington, DE, USA) in order to determine RNA concentration and purity. A high capacity cDNA archive kit (Applied Biosystems) was used to reverse transcribe the equalized RNA samples. Quantitative RT-PCR was performed with 50 ng cDNA using custom-designed gene-expression assays for PGAM1 and CRIP1a.

The gene expression of the targets was assessed using Taqman gene expression assays (Applied Biosystems) containing specific target primers and FAM-labelled MGB target probes. Analysis was performed using the ΔΔCT method. The primers used are shown in Fig 8.

Western blot analysis

For western blot analysis, 500 μm thick sections of each brain were generated using a vibratome (Leica Microsystems, GmbH, Germany), and the hippocampal area was subdissected using a surgical blade. Hippocampal tissues were homogenized in 50 mM PBS (pH 7.4), containing 0.1 mM ethylene glycol-bis(2-aminoethylether)-N,N,N′ ,N′ -tetraacetic acid (pH 8.0); 0.2% Nonidet P-40; 10 mM ethylenediaminetetraacetic acid (pH 8.0); 15 mM sodium pyrophosphate; 100 mM β-glycerophosphate; 50 mM NaF; 150 mM NaCl; 2 mM sodium orthovanadate; 1 mM phenylmethylsulfonyl fluoride; and 1 mM DTT. After centrifugation, protein levels in the supernatants were determined using a Micro BCA protein assay kit according to the manufacturer's instructions (Pierce Chemical, Rockford, IL, USA). Aliquots containing 20 μg of total protein were denatured by boiling in loading buffer containing 150 mM Tris (pH 6.8), 3 mM DTT, 6% sodium dodecyl sulphate, 0.3% bromophenol blue, and 30% glycerol. Each aliquot was loaded onto a polyacrylamide gel. After electrophoresis, proteins were transferred to nitrocellulose membranes (Pall Crop, East Hills, NY, USA), which were then blocked in 5% non-fat dry milk in PBS/0.1% Tween 20 for 45 minutes, prior to incubation with a peroxidase-conjugated rabbit anti-CRIP1 antibody (diluted 1:1,000, Abcam, Cambridge, UK). Detection was performed using the peroxidase-conjugated IgG and an enhanced luminol-based chemiluminescent kit (Pierce Chemical). The blots were scanned, and densitometry was performed, using Scion Image software (Scion Corp., Frederick, MD,

USA). Blots were stripped and reprobed with an antibody against β-actin as an internal loading control. Data were normalized to the β-actin level in each lane.

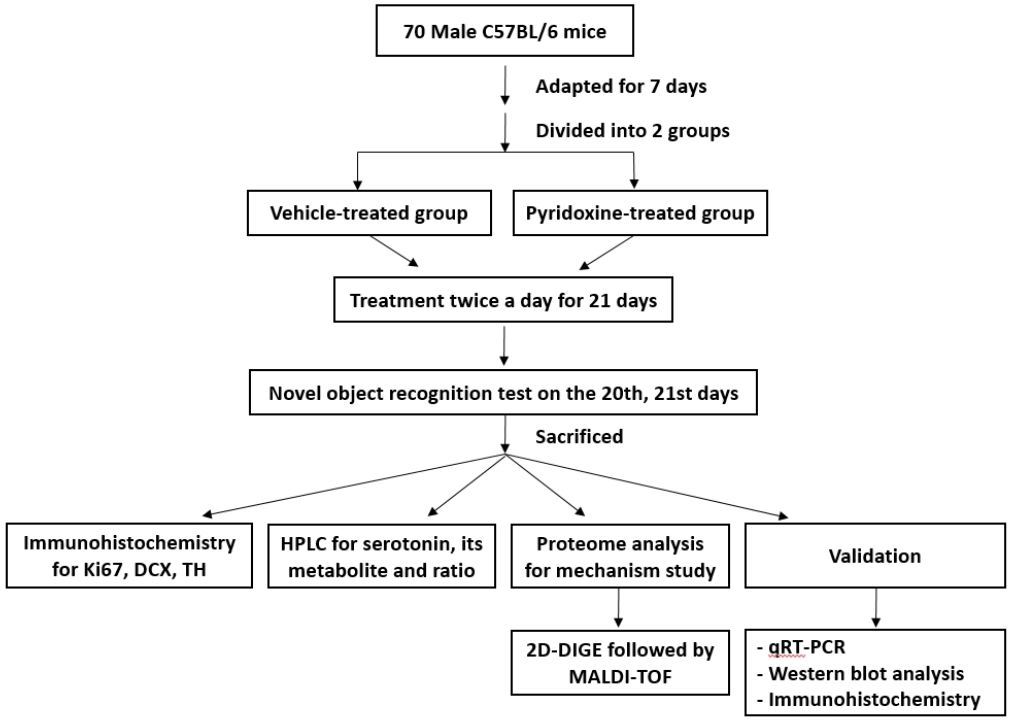

Figure 1. Schematic workflow of experimental design 1.

Experimental design 2

In the experimental design 2, we conducted two experiments on CRIP1a that was identified in the proteomic analysis in the experiment design 1. One is about the role of CRIP1a in the hippocampal functions and the other is about the effects of CB1 receptor blocking.

Effect of CRIP1a on the hippocampal functions

Experimental animals

Male C57BL/6J mice (7 weeks of age, n=10) were purchased from Jackson Laboratory Co. Ltd (Bar Harbor, ME, USA). They were housed under standard conditions with feasible temperature (22 ± 2ºC) and humidity (60 ± 5%) control and a 12:12 h light/dark cycle with ad libitum access to food and water. The handling and care of the animals conformed to National Institutes of Health Guidelines for the Care and Use of Laboratory Animals, NIH Publication No. 85-23, 1985, revised 1996). Animal procedures were approved by the Institutional Animal Care and Use Committee (IACUC) of Seoul National University. The animals were divided into 2 groups: CRIP1a siRNA-treated, scramble-treated group.

Knockdown of CRIP1a in the hippocampus

Mice were anesthetized with a mixture of 2.5% isoflurane (Baxtor, Deerfield, IL) in 33% oxygen and 67% nitrous oxide and received bilateral injections of Accell SMARTpool siRNAs (GE Healthcare Dharmacon, Lafayette, CO, USA) targeting CB1

cannabinoid receptor-interacting protein 1a (CRIP1a, #E-063624-00-0050) or a negative control into the dorsal hippocampus using stereotaxic coordinates (+2.0 mm anteroposterior, ± 1.6 mm mediolateral, −1.3 mm dorsoventral relative to bregma (Franklin and Paxinos, 1997). The infusion was given over a 10-min period (0.1 μL/min) for a total volume of 1 μL per side. Fresh Accell siRNA stocks (100 μM) were resuspended in Accell siRNA resuspension buffer to a concentration of ~4.5 μM on the day of surgery.

Novel object recognition test

On the 48th day of CRIP1a siRNAs or negative control treatment (1 h after treatment), mice of each group (n = 10 per group) were allowed to explore the apparatus for 2 min. On the testing day (49th day of treatment), novel object recognition test was conducted as described previously.

Confirmation of CRIP1a down-regulation in the hippocampus

To confirm the effects of siRNA targeting CRIP1a within the hippocampus, animals were euthanized at 7 weeks following the treatment (n = 5 per group) and their brains removed. Western blot analysis was conducted as described previously.

Tissue processing and immunohistochemistry

To observe the effects of CRIP1a knockdown on the expressional confirmation, cell proliferation, and neuroblast differentiation, immunohistochemical staining was conducted for identification of CRIP1, Ki67, and doublecortin (DCX), respectively, as

described previously. Briefly, animals (n = 5 per group) were anesthetized with 1 g/kg urethane (Sigma-Aldrich, St. Louis, MO) at 7 weeks after treatment. Serial coronal brain sections (30 μm) were incubated with a rabbit anti-CRIP1 antibody (1:200, Novus Biologicals, Littleton, CO, USA); rabbit anti-Ki67 antibody (1:1,000; Abcam); or goat anti-DCX antibody (1:50; Santa Cruz Biotechnology, Santa Cruz, CA, USA) overnight at room temperature. Sections were then incubated with biotinylated goat anti-rabbit IgG, followed by a streptavidin-peroxidase complex (1:200, Vector, Burlingame, CA, USA). Immunostaining was visualized by reaction with DAB in 0.1 M Tris-HCl buffer (pH 7.2). Sections were dehydrated and mounted on gelatin-coated slides in Canada balsam (Kanto, Tokyo, Japan).

Effects of CB1 receptor blocking and/or pyridoxine on cell proliferation and neuroblast differentiation

Inhibition of CB1 cannabinoid receptor

The mice were divided into four groups (n = 14 in each group): vehicle (physiological saline)-treated, pyridoxine-treated, rimonabant (a CB1 cannabinoid receptor antagonist, Sigma)-treated, and pyridoxine hydrochloride (Sigma) with rimonabant-treated. Vehicle or pyridoxine was intraperitoneally administered to the mice at 8 weeks of age, twice a day for 3 weeks, as described in section 2.2. In addition, 10 mg/kg rimonabant was administered orally to the mice every 3 weeks, as this protocol is known to show central effects, such as loss of antidepressive activity by imipramine, in mice (Lee et al., 2009).

Novel object recognition test

On the 20th day of vehicle administration, mice treated with pyridoxine, and/or rimonabant treatment (1 h after treatment), mice (n = 7 per group) were allowed to explore the apparatus for 2 min. On the testing day (21st day of treatment), a novel object recognition test was conducted as described previously.

Tissue processing and immunohistochemistry

To observe the effects of CB1 receptor blocking and/or pyridoxine on dopamine synthesis, cell proliferation, and neuroblast differentiation, an immunohistochemical study was conducted for TH, Ki67, and DCX, respectively, as described previously.

Quantification of serotonin and its metabolite by HPLC

To observe the effects of CB1 receptor blocking and/or pyridoxine on serotonin turnover, mice (n = 7 per group) used in the novel object recognition test were sacrificed and the concentrations of 5-HT and 5-hydroxyindoleacetic acid (5-HIAA) in hippocampal homogenates were measured using HPLC, as described previously.

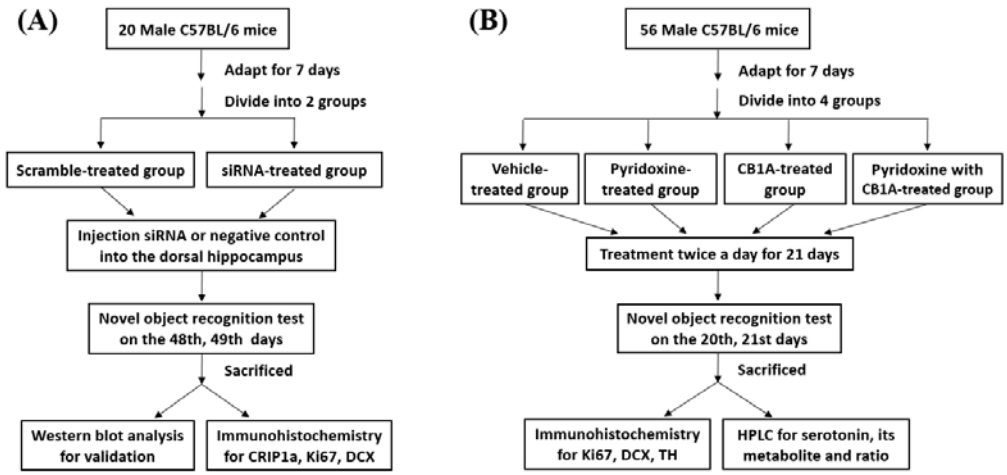

Figure 2. Schematic workflow of experimental design 2.

Expreimental design 3

In the experimental design 3, we investigated the effects of PGAM1 on novel object recognition, cell proliferation, and neuroblast differentiation in the mouse dentate gyrus. Experimental animals were divided into 4 groups: control, Tat peptide-, control-PGAM1-, and Tat-PGAM1-treated group.

Experimental animals

Male C57BL/6J mice (7 weeks of age, n = 40) were purchased from Jackson Laboratory Co. Ltd (Bar Harbor, ME, USA). Five animals were housed per cage in a conventional area under standard conditions at ambient temperature (22 ± 2ºC) and humidity (60 ± 5%) on a 12/12 h light/dark cycle with ad libitum access to food and water. Animal handling and care conformed to the guidelines of current international laws and policies (National Institutes of Health Guide for the Care and Use of Laboratory Animals, Publication No. 85–23, 1985, revised 1996) and were approved by the Institutional Animal Care and Use Committee of Seoul National University (SNU-170417-19-1). All experiments were conducted with an effort to minimize the number of animals used and the physiological stress caused by the procedures employed. All experimental procedures were conducted according to ARRIVE guidelines [34].

Construction of expression vectors

A cell-permeable Tat expression vector was prepared in the laboratory as previously described (Stenfors and Ross, 2002). The cDNA sequence of human PGAM1 was amplified by polymerase chain reaction (PCR) using the PGAM1 specific sense primer 5'

CTC GAG ATG GCC GCC TAC A 3' and the PGAM1 specific anti-sense primer 5' GGA TCC TCA CTT CTT GGC CTT 3'. PCR products were excised, eluted (Expin Gel; GeneAll Biotechnology Co., Ltd., Seoul, Korea), and ligated into a TA cloning vector (pGEM® T easy vector; Promega Corporation, Madison, WI, USA) according to the manufacturer's protocol. The purified TA vector containing human PGAM1 cDNA was ligated into the Tat expression vector to produce a Tat-PGAM1 fusion protein. The recombinant expression plasmid consisted of 6His-Tat-PGAM1 in a pET-15 vector. We also constructed 6His-PGAM1 without Tat as a control. To produce the Tat-PGAM1 and control-PGAM proteins, the plasmid was transformed into Escherichia coli BL21 cells. The transformed bacterial cells were grown in 100 mL of lysogeny broth media to a D600 value of 0.5–1.0 and then induced with 0.5 mM isopropyl β D 1 thiogalactopyranoside at 18ºC for 18 h. Harvested cells were lysed by sonication and purified using a Ni2+ nitrilotriacetic acid Sepharose affinity column (Qiagen, Inc.) and PD 10 column chromatography (GE Healthcare, Chicago, IL, USA). The concentration of purified proteins was estimated using a Bradford assay (Lesch et al., 1996). Equal amounts of protein were analyzed using 10% sodium dodecyl sulfate polyacrylamide gel electrophoresis (SDS-PAGE). Proteins were then electrotransferred to a polyvinylidene difluoride membrane. The membrane was blocked with tris-buffered saline (25 mM Tris-HCl, 140 mM NaCl, 0.1% Tween 20, pH 7.5) containing 5% non-fat dry milk and subsequently probed using anti-polyhistidine antibodies (1:2,000, His-probe, SantaCruz Biotechnology, Santa Cruz, CA, USA). Proteins were identified using chemiluminescent reagents as recommended by the manufacturer (Amersham, Franklin Lakes, NJ, USA).

Administration of Tat-PGAM1

Following a 1-week acclimation to laboratory conditions, mice were divided into 4

groups (n = 10 in each group): control, Tat peptide-, control-PGAM1-, and Tat-PGAM1-treated groups. Tat peptide (2 mg/kg), control-PGAM1, and Tat-PGAM1 (10 mg/kg) were intraperitoneally administered to mice at 8 weeks of age, once a day for 3 weeks.

Novel object recognition test

On the 20th day of treatment with control, Tat peptide, control-PGAM1-, or Tat-PGAM1, 1 h after treatment, mice from each group (n = 10 per group) were allowed to explore the apparatus for 2 min. On the testing day (21st day of treatment), novel object recognition test was conducted as described previously.

Confirmation of Tat-PGAM1 delivery into hippocampus

To confirm the effects of Tat-PGAM1 within the hippocampus, animals were euthanized at 7 weeks following the treatment (n = 5 per group) and their brains removed. Western blot analysis was conducted as described previously.

Tissue processing and immunohistochemistry

To observe the effects of CB1 receptor blocking and/or pyridoxine on dopamine synthesis, cell proliferation, and neuroblast differentiation, an immunohistochemical study was conducted for Ki67, DCX, and p-CREB respectively, as described previously.

Data analysis

Tissue sections between 1.46 mm and 2.46 mm posterior to the bregma were selected

by referring to the mouse atlas by Franklin and Paxinos (Franklin and Paxinos, 1997). A total of 5 sections per animal, 90 μm apart from each other, were used for analysis of immunohistochemical data.

Measurement of cell number

Sections taken in the hippocampal dentate gyrus region were examined using an image analysis system and ImageJ software v. 1.5 (National Institutes of Health, Bethesda, MD, USA). Digital images of the mid-point of the hippocampal dentate gyrus were captured with a BX51 light microscope (Olympus, Tokyo, Japan) equipped with a digital camera (DP72, Olympus) connected to a computer monitor. Images were calibrated into an array of 512 × 512 pixels corresponding to a tissue area of 1200 μm × 900 μm (100× primary magnification). Each pixel resolution was 256 gray levels, and the intensity of DCX, and TH immunoreactivity was evaluated by relative optical density (ROD), which was obtained after transformation of the mean gray level using the formula: ROD = log(256/mean gray level). The ROD of background staining was determined in unlabeled portions of the sections using Photoshop CC software (Adobe Systems Inc., San Jose, CA, USA), and this value was subtracted to correct for nonspecific staining, using ImageJ v. 1.50 software (National Institutes of Health). Data are expressed as a percentage of the vehicle-treated group values (set to 100%).

Measurement of cell number

Ki67- and pCREB-positive cell counts were performed for each section of the dentate gyrus using an image analysis system equipped with a computer-based CCD camera (software: Optimas 6.5, CyberMetrics, Scottsdale, AZ, USA). Cell counts from all of the

sections of all of the mice were averaged.

Statistical analysis

The data shown here represent the means ± the standard error of the mean (SEM). Differences among means were statistically analyzed using the one-way ANOVA test, followed by Bonferroni post-hoc tests, or Student t-test. Statistical significance was considered at $P < 0.05$.

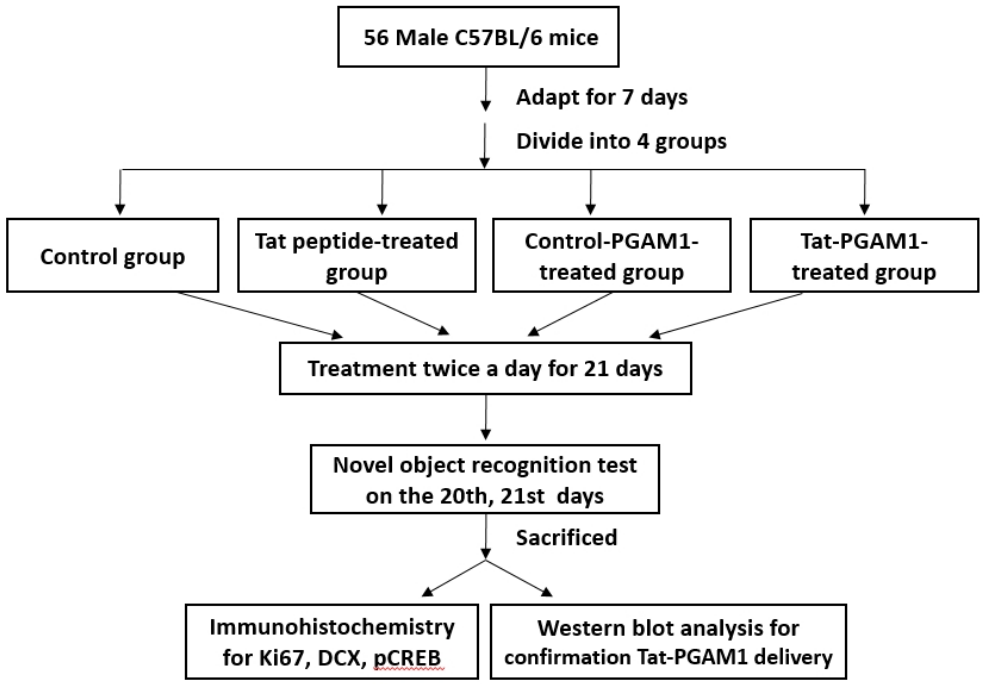

Figure 3. Schematic workflow of experimental design 3.

Results

Experimental design 1

Effects of pyridoxine on novel object recognition memory

In both the vehicle- and pyridoxine-treated groups, no significant differences were observed in the amount of time spent exploring two identical objects during the training period. During the testing period, mice in both treatment groups spent more time exploring the new object than they did the familiar object. The pyridoxine-treated mice spent more time exploring the new object than did the vehicle-treated mice, although this difference was not significant. However, the discrimination index was considerably higher in the pyridoxine-treated group than in the vehicle-treated group (Fig 4).

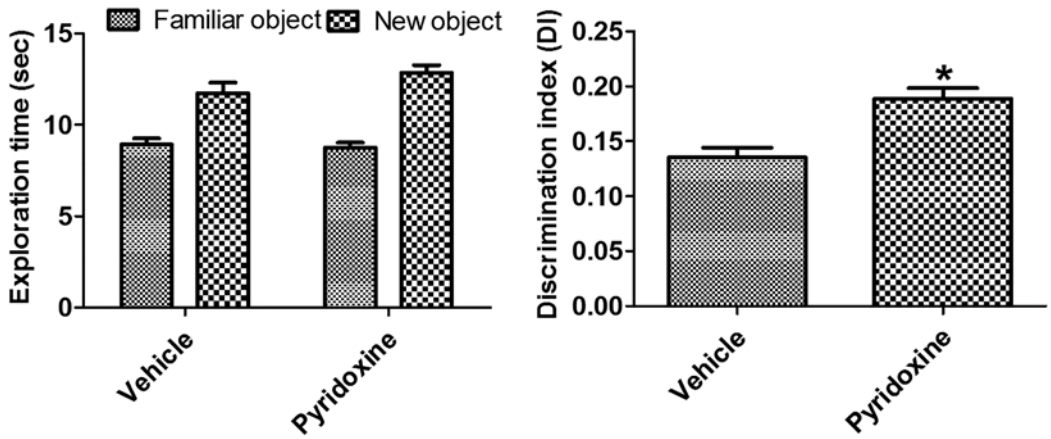

Fig 4. Pyridoxine improves novel object recognition memory. Effect of vehicle and pyridoxine on exploration time and discrimination index of familiar vs. novel objects during a novel object recognition test in mice (n = 20 per group; $*p < 0.05$). Data for exploration time for each object (same one, where one object was replaced by a new one on the testing day) are presented as a percentage of total exploration time. All data are shown as % exploration time ± SEM.

Turnover of 5-HT and changes in TH immunoreactivity in vehicle- and pyridoxine-treated groups

Turnover of 5-HT

The levels of 5-HT and 5-HIAA in hippocampal homogenates from the vehicle-treated group were 0.41 ± 0.032 and 0.65 ± 0.033 ng/mg protein, respectively. The ratio of 5-HIAA/5-HT was 1.59. In the pyridoxine-treated group, levels of 5-HT in hippocampal homogenates were increased, while 5-HIAA levels were decreased, relative to those of the vehicle-treated group, although this difference was not significant. However, the ratio of 5-HIAA/5-HT was significantly lower in the pyridoxine-treated group than in the vehicle-treated group (Fig 5).

Changes in TH immunoreactivity

In the vehicle-treated group, TH immunoreactive fibers were found in the molecular layer and polymorphic layer of the dentate gyrus. In the pyridoxine-treated group, TH immunoreactive fibers were more abundant in the dentate gyrus compared with the vehicle-treated group. In the pyridoxine-treated group, TH immunoreactivity was significantly increased by 195.9% of that observed in the vehicle-treated group (Fig 5).

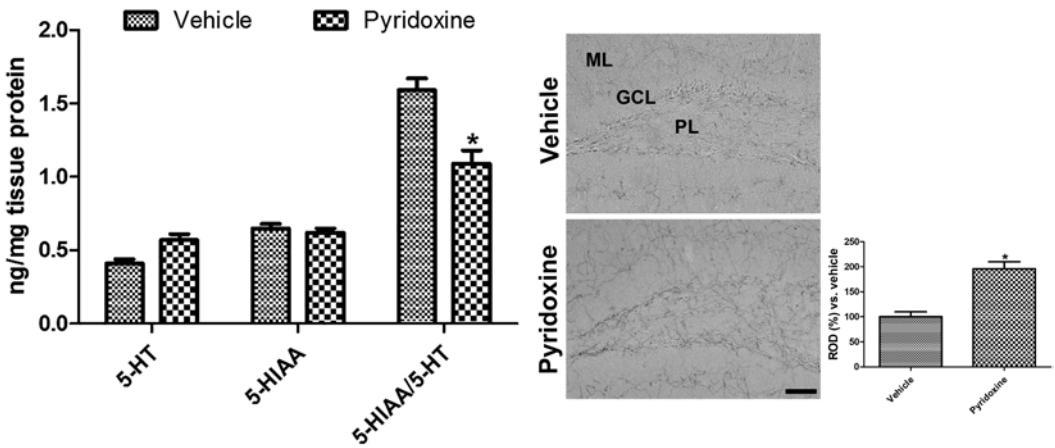

Fig 5. Pyridoxine increases serotonin turnover and TH immunoreactivity. Effect of pyridoxine on levels of serotonin (5-hydroxytryptamine, 5-HT), its metabolite (5-hydroxyindoleacetic acid, 5-HIAA), and ratio (5-HIAA/5-HT) in the vehicle- and pyridoxine-treated groups (n = 5 mice per group; **P* < 0.05, versus vehicle-treated group). All data are shown as the ratio to vehicle-treated group ± SEM. Immunohistochemistry for TH in the dentate gyrus of vehicle- and pyridoxine-treated mice. Scale bar = 50 μm. The ROD values, expressed as a percentage of the value of the TH immunoreactivity in the dentate gyrus of the vehicle-treated group, are also shown (n = 5 mice per group; **P* < 0.05, versus vehicle-treated group). The values are expressed as mean ± SEM. ROD: relative optical density; SEM: standard error of the mean; TH: tyrosine hydroxylase.

Protein identification by 2D-DIGE followed by MALDI-TOF MS in the hippocampus

Approximately 2,690 spots were detected using the in-gel module of DeCyder Analysis Software module using a pH range of 3 to 10. Three spots were differentially distributed with at least 1.5-fold volume changes between the vehicle- and pyridoxine-treated hippocampal homogenates. The master gel spots were visualized using CBB-stained preparative gels and selected for identification analysis (Fig 6). In 3 separate gels, a total of 27, 45, and 45 protein spots changed more than 1.5-fold. However, only 3 overlapping protein spots were observed in each gel.

The three differentially distributed spots were identified as two known proteins and one unknown protein using the SWISS-PROT and NCBInr databases. Search results were evaluated on the basis of accepted standards that take into account the number of peptides matched to the candidate protein, the difference in the number of matched peptides between candidate proteins and the next best fit, and the coverage of candidate protein sequences by matching peptides of the experimental and theoretical pI and Mr values (Jensen et al., 1999). The results of MALDI-TOF MS analysis for the identified spots are listed in Fig 5. The proteins identified were phosphoglycerate mutase 1 (PGAM1), CRIP1, and a protein that did not match any listed in the databases, as shown in Fig 4. The standard abundance values of PGAM1 and the unnamed protein were significantly higher, while those of CRIP1 were significantly lower, in the pyridoxine-treated group than in the vehicle-treated group (Fig 7).

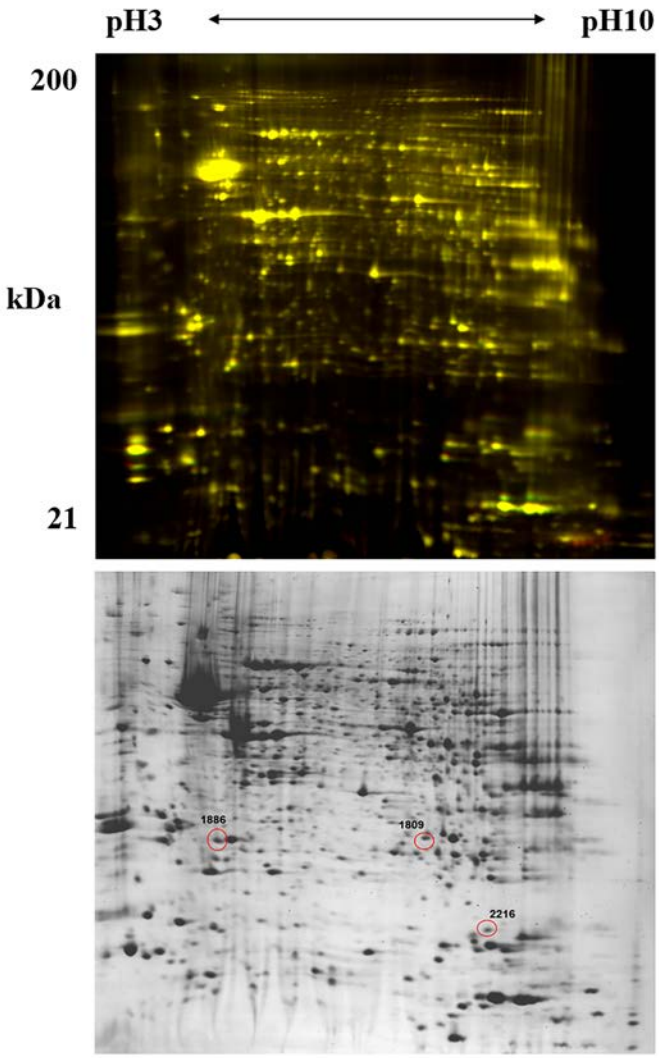

Fig 6. 2D-DIGE proteomes. Two dimensional-fluorescence difference gel electrophoresis (DIGE) gel (upper panel) of hippocampal proteins labelled with CyDye™ fluors was performed to compare the proteomes from vehicle- and pyridoxine-treated groups Master gels (lower panel) were used to pick the spots for analysing the data with MALDI-TOF MS. Gel images of the three selected proteins included in each panel. MALDI-TOF MS: matrix-assisted laser desorption/ionization time-of-flight mass spectrometry.

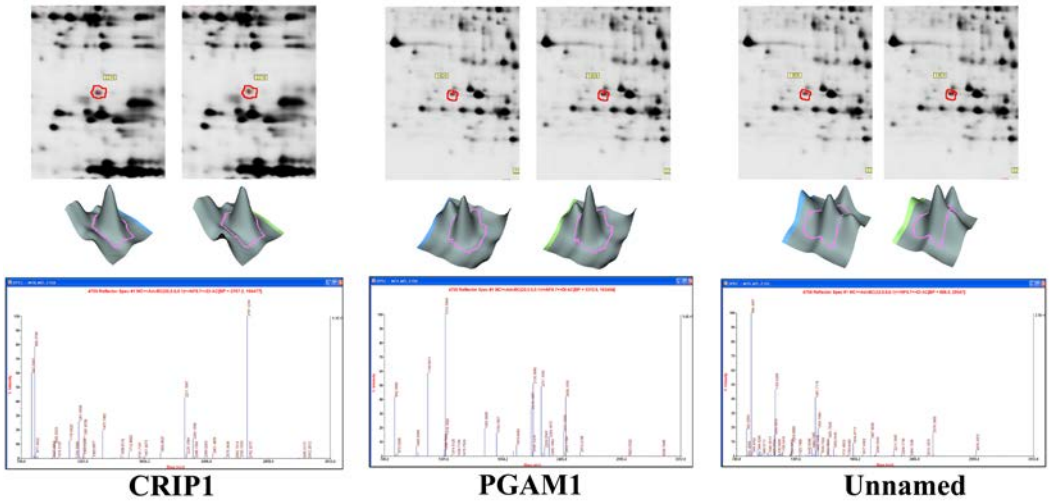

Table 1. Changed proteins in hippocampal homogenates between vehicle- and pyridoxine-treated animals

Proteins (gI accession number)	Number of peptides matched in the identified protein	Percentage covering of the matched peptides (%)	pI, Mr (kDa)	MOWSE	Fold increase/decrease	P values
phosphoglycerate mutase 1 (114326546)	14	52	6.67, 28.8	141	1.96	0.0007
Unnamed protein (26344461)	12	28	8.47, 58.4	66	1.55	0.0025
CB1 cannabinoid receptor-interacting protein 1 (62000629)	9	59	7.74, 18.6	77	-1.54	0.0004

Fig 7. Identification of differentially expressed proteins. Enlarged view of DIGE gels (upper panel). Each panel shows an enlarged view of differentially expressed gel spots from DIGE gels. Three-dimensional representations of spot volumes were derived from differentially expressed proteins. Graphical representations of all matched spots for a particular protein are shown in the middle panels (dots were plotted with two independent values from the three gels in which vehicle- and pyridoxine-treated samples were run). Peptide mass fingerprints of three spots are also shown, along with a summary of protein properties as identified using MALDI (lower panel). DIGE: fluorescence difference gel electrophoresis; MALDI: matrix-assisted laser desorption/ionization.

Validation of identified materials by qRT-PCR, western blot and/or immunohistochemical analyses

qRT-PCR, western blot

To validate the identity of differentially expressed proteins in the hippocampal homogenates, qRT-PCR analysis was conducted owing to difficulties in obtaining commercially available antibodies against PGAM1. CRIP1a mRNA in the hippocampal homogenates of the pyridoxine-treated group was significantly decreased to 39.4% of that in the vehicle-treated group. In addition, the CRIP1a protein levels were significantly decreased to 58.1% of that in the vehicle-treated group. In contrast, PGAM1 mRNA in the pyridoxine-treated group was significantly increased to 299% of that in the vehicle-treated group (Fig 8).

Immunohistochemistry

In both the vehicle- and pyridoxine-treated groups, CRIP1 immunoreactive structures were found in the stratum pyramidale of the hippocampal CA1 and CA3 regions, as well as the granule cell layer of the dentate gyrus. However, CRIP immunoreactivity in the pyridoxine-treated group was decreased in the hippocampal CA1 region and dentate gyrus compared with the vehicle-treated group (Fig 8).

Gene	Forward primer	Reverse primer
CRIP1a	5′-aatttctagaGCCACCATGGGGGACCTACCC-3′	5′-ggccaagcttTCAGAGGAAGGACTCCTTATTCACCCA-3′
PGAM1	5′-ATGCTAAGCCATGACCAGTGAG-3′	5′-ATCACCACGCAGGTTACATTCG-3′
GAPDH	5′-CAAAATGGTGAAGGTCGGTGTG-3′	5′-TGATGTTAGTGGGGTCTCGCTC-3′

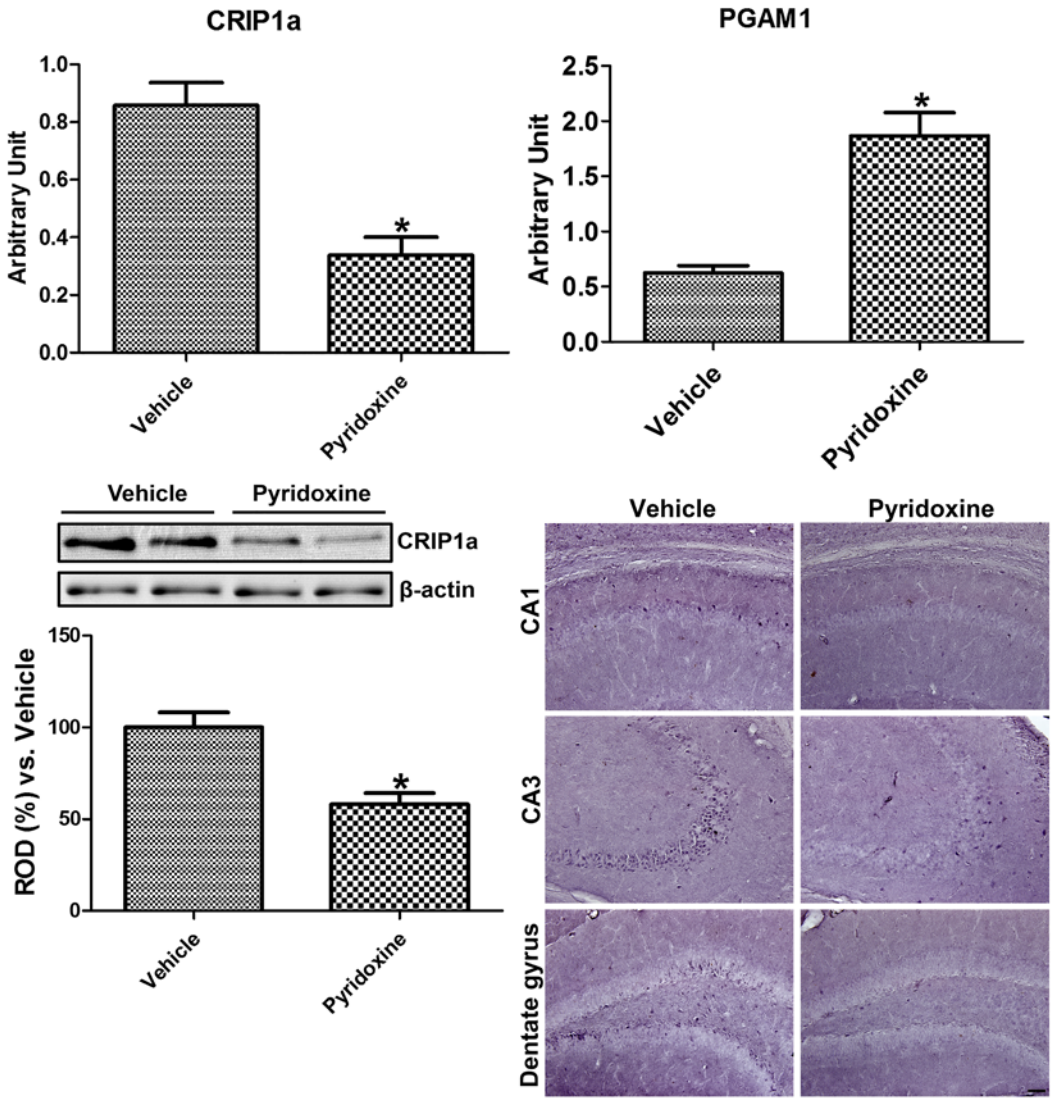

Fig 8. Quantitative RT-PCR validation of differentially expressed proteins as well as western blot and immunohistochemical validation of CRIP1a. List of primers used in qRT-PCR experiments and quantitative analysis of mRNA to validate the differential expression of CRIP1a and PGAM1 in the hippocampi of vehicle- vs. pyridoxine-treated mice (n = 5 per group; $*P < 0.05$, versus vehicle-treated group). Western blot analysis of CRIP1a protein in the hippocampi of vehicle- vs. pyridoxine-treated mice (n = 5 per group; $*P < 0.05$, versus vehicle-treated group). All data are shown as the ratio to vehicle-treated group ± SEM. Immunohistochemistry for CRIP1 in the hippocampal CA1, CA3, and dentate gyrus of vehicle- and pyridoxine-treated mice. Scale bar = 50 μm. CRIP1a: cannabinoid receptor-interacting protein 1a; PGAM1: phosphoglycerate mutase 1; SEM: standard error of the mean.

Experimental design 2

Effects of CRIP1a siRNA on novel object recognition memory, cell proliferation, and neuroblast differentiation

To investigate the role of CRIP1a on hippocampal neurogenesis, we administered scramble or CRIP1a siRNA into the hippocampus. Western blot data showed that CRIP1a significantly reduced in the CRIP1a siRNA-treated group to 64.2% of the scramble-treated group (Fig 9). In addition, administration of CRIP1a siRNA showed a significantly higher discrimination index compared to that of the scramble-treated group, although there was no significant difference in time spent exploring the new object (Fig. 10). Furthermore, the number of Ki67-positive proliferating cells was significantly increased in the CRIP1a siRNA-treated group by 220% of that observed in the scramble-treated group. DCX-immunoreactive neuroblasts were more prominently observed in the CRIP1a siRNA-treated group than in the scramble-treated group. In the CRIP1a siRNA-treated group, DCX immunoreactivity was significantly higher by 158.2% than that observed in the scramble-treated group (Fig 11).

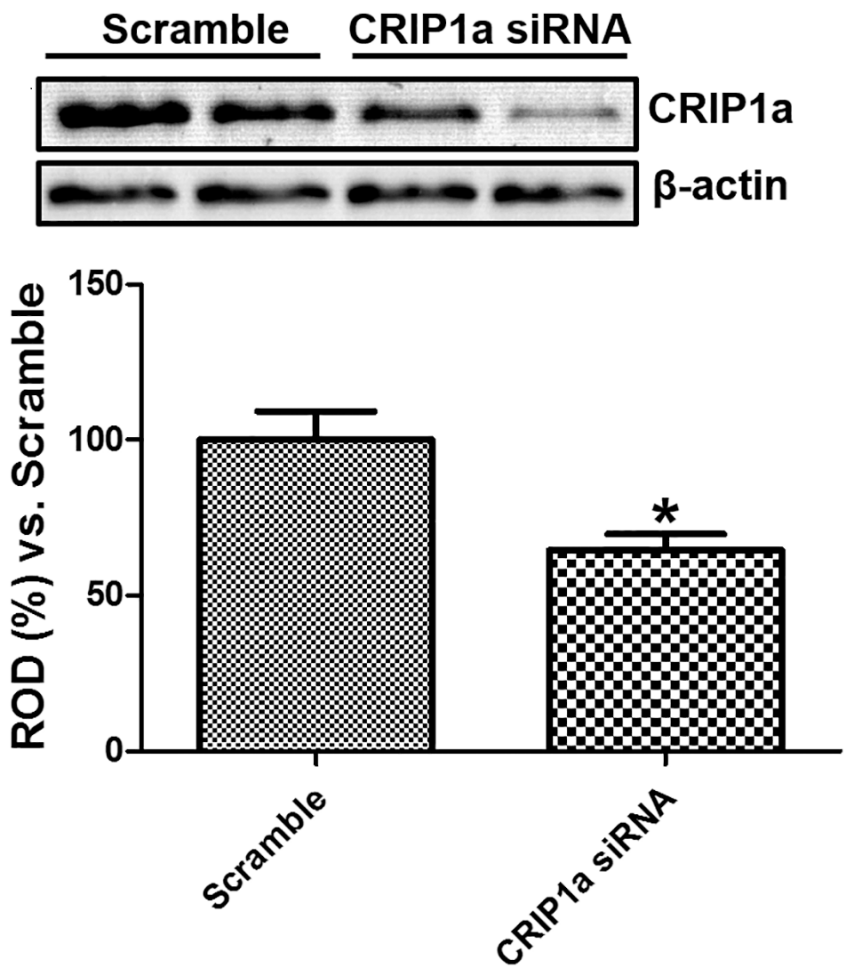

Fig 9. Effects of CRIP1a knockdown in the mouse. Western blot validation of CRIP1a reduction in the hippocampi of scramble vs. CRIP1a siRNA-treated mice (n = 5 per group; *P < 0.05, versus vehicle-treated group). Data are shown as the ratio to vehicle-treated group ± SEM.

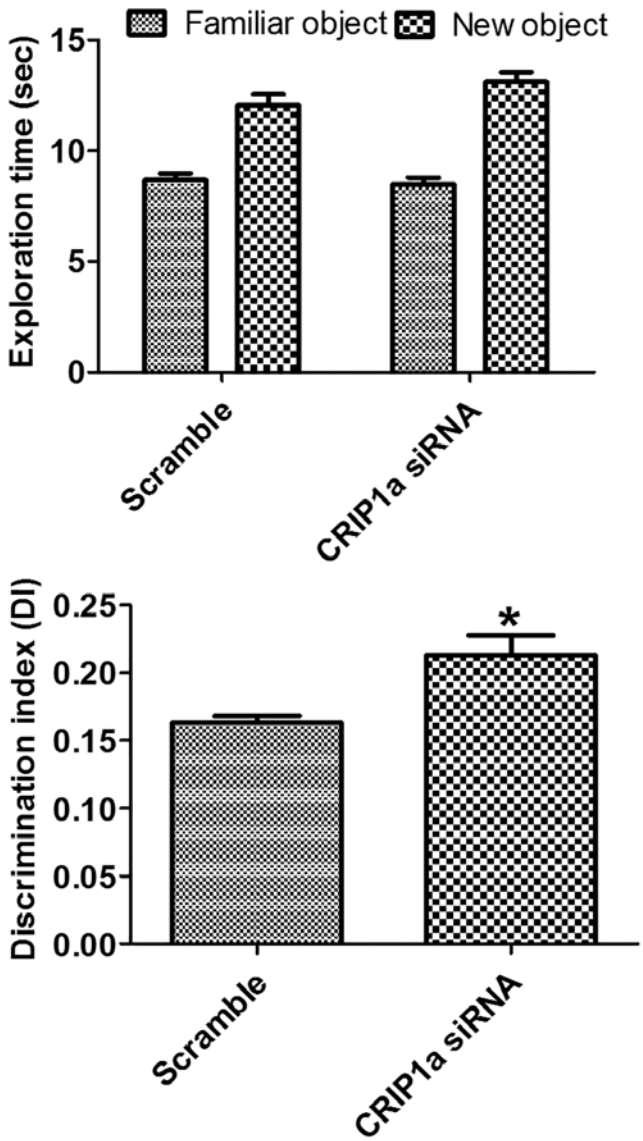

Fig 10. Effect of scramble and CRIP1a siRNA on exploration time and discrimination index of familiar vs. novel objects during a novel object recognition test in mice (n = 5 per group; *$p < 0.05$). Data for exploration time for each object (same one, where one object was replaced by a new one on the testing day) are presented as a percentage of total exploration time. All data are shown as % exploration time ± SEM.

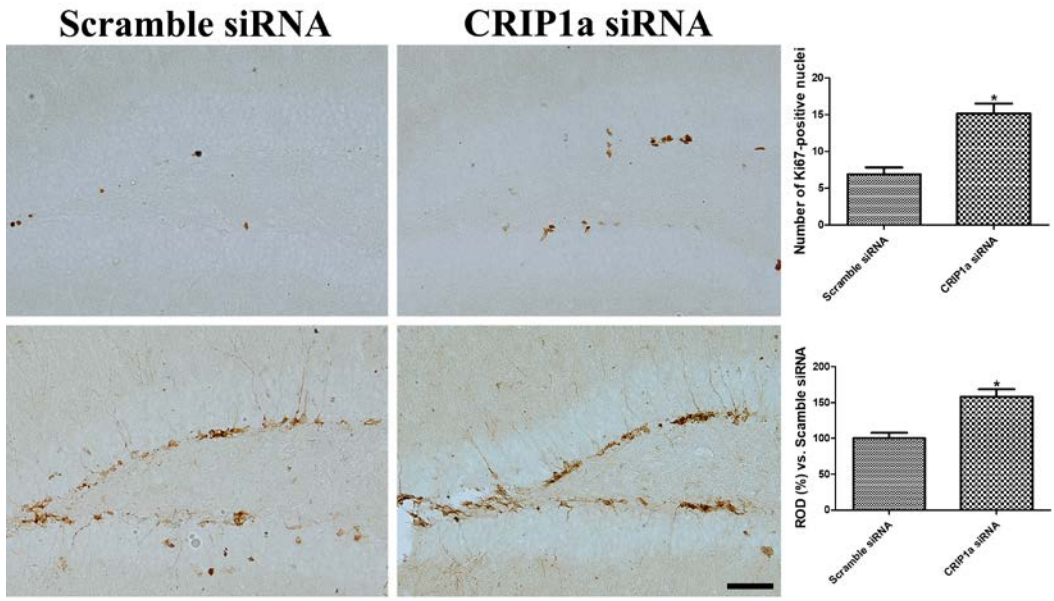

Fig 11. Immunohistochemistry for Ki67 and DCX in the dentate gyrus of scramble vs. CRIP1a siRNA-treated mice. Scale bar = 50 μm. The number of Ki67-positive nuclei per section for each group, and the ROD expressed as a percentage of the value of the DCX immunoreactivity in the dentate gyrus of the vehicle-treated group, are also shown (n = 5 mice per group; **P* < 0.05, versus scramble-treated group). Data are presented as mean ± SEM. CRIP1a: cannabinoid receptor-interacting protein 1a; DCX: doublecortin; ROD: relative optical density; SEM: standard error of the mean.

Effects of CB1 cannabinoid receptor antagonist on hippocampal functions

Novel object recognition memory

During the training period, there were no significant differences in the amount of time spent exploring two identical objects in all of the experimental groups. During the testing period, vehicle-treated and pyridoxine-treated mice spent significant more time exploring the new object than they did the familiar object. Rimonabant-treated mice also spent more time exploring the new object than did the vehicle-treated mice, although no statistical difference was observed for the difference in the amount of time spent on familiar compared with new objects. However, pyridoxine treatment with rimonabant significantly increased the time spent on the new object compared with time spent on the familiar one. The discrimination index significantly increased in the pyridoxine-treated group compared with the vehicle-treated group. The discrimination index was significantly decreased in the rimonabant-treated group compared with the vehicle- or pyridoxine-treated groups. Pyridoxine treatment ameliorated the reduction of the discrimination index by rimonabant to levels comparable with those in the vehicle-treated group (Fig 12).

Turnover of 5-HT and changes in TH immunoreactivity

No significant changes in the levels of 5-HT and 5-HIAA in the hippocampal homogenates were observed among the groups, although 5-HT levels were higher in the pyridoxine-treated group and lower in the rimonabant-treated group. However, the ratio of 5-HIAA/5-HT significantly decreased in the pyridoxine-treated group compared with the other groups (Fig 13).

TH immunoreactivity was significantly higher in the dentate gyrus of pyridoxine-treated group than in the vehicle-treated group. In the rimonabant-treated group, TH immunoreactivity was significantly decreased in the dentate gyrus compared with the vehicle-treated group. Pyridoxine treatment ameliorated the rimonabant-induced reduction of TH immunoreactivity in the dentate gyrus although no statistical significance was detected (Fig 14).

Cell proliferation and neuroblast differentiation

To investigate the role of a CB1 cannabinoid receptor antagonist with or without pyridoxine on cell proliferation and neuroblast differentiation, we orally administered rimonabant, a CB1 cannabinoid receptor antagonist, to mice with or without pyridoxine treatment. Pyridoxine administration significantly increased the numbers of Ki67-positive nuclei and DCX-immunoreactive neuroblasts in the dentate gyrus compared with the vehicle-treated group. In the rimonabant-treated group, the numbers of Ki67-positive nuclei and DCX-immunoreactive neuroblasts were significantly lower than in the vehicle-treated group. Pyridoxine treatment slightly increased the rimonabant-induced reduction of Ki67-positive nuclei and DCX-immunoreactive neuroblasts, although no statistical significance was detected (Fig 14).

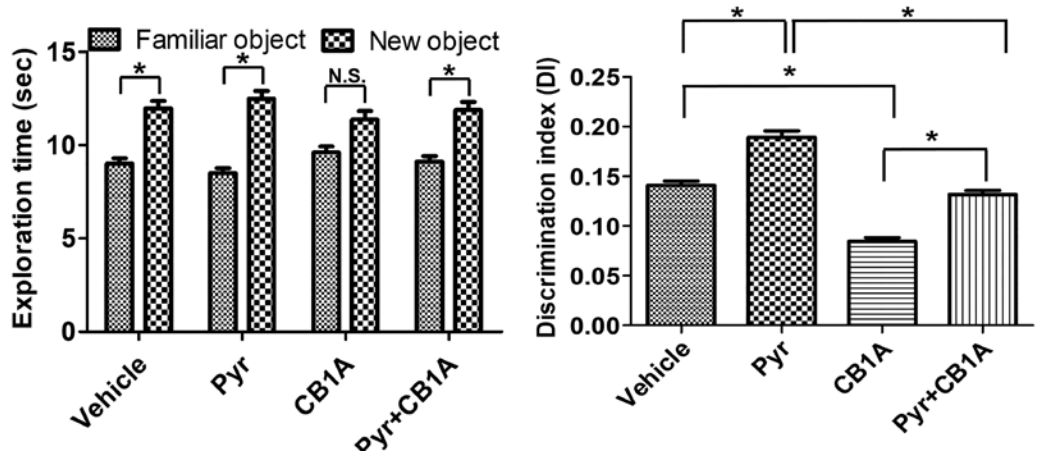

Fig 12. Effect of CB1R inhibition and/or pyridoxine on exploration time and discrimination index of familiar vs. novel objects during a novel object recognition test in mice (n = 7 per group; $*p < 0.05$). Data for exploration time for each object (same one, or new one where one object was replaced by a new one on the testing day) are presented as a percentage of total exploration time. All data are shown as % exploration time ± SEM.

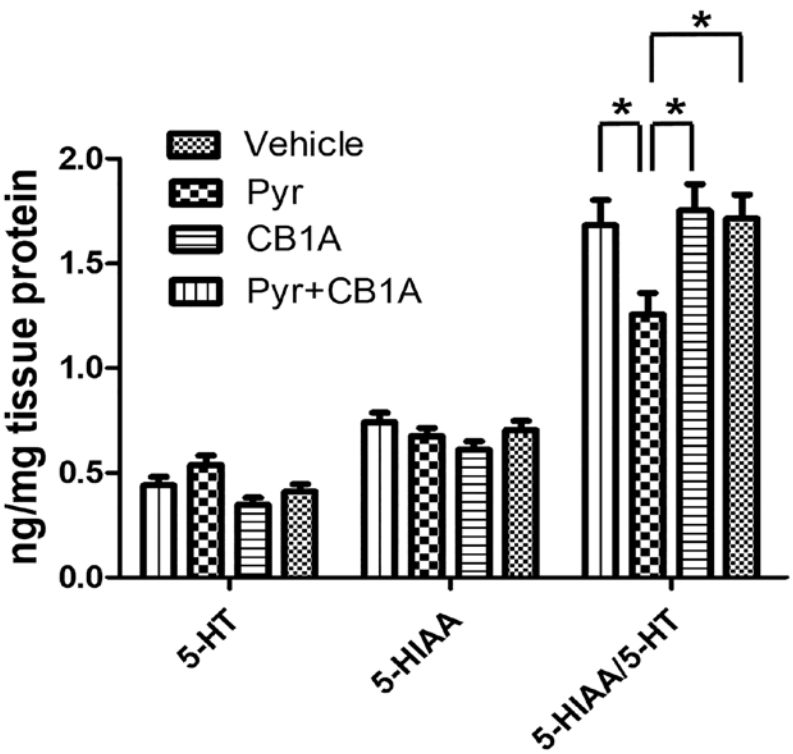

Fig 13. Effect of pyridoxine on levels of serotonin (5-hydroxytryptamine, 5-HT), its metabolite (5-hydroxyindoleacetic acid, 5-HIAA), and ratio (5-HIAA/5-HT) in the vehicle-, Pyr-, CB1A-, and Pyr+CB1A-treated groups (n = 7 mice per group; *$P < 0.05$, versus vehicle-treated group). All data are shown as the ratio to vehicle-treated group ± SEM.

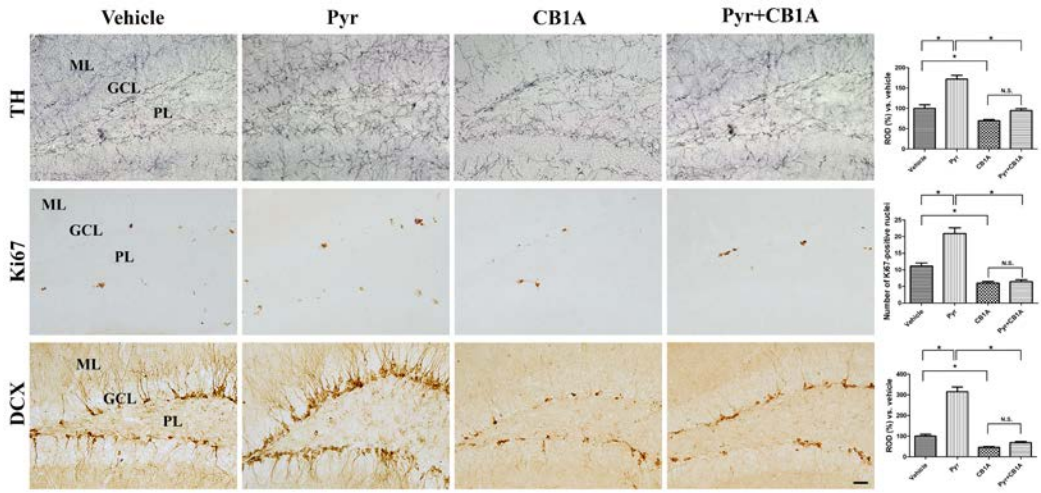

Fig 14. Immunohistochemistry for TH, Ki67, and DCX in the dentate gyrus of vehicle-, Pyr-, CB1A-, and Pyr+CB1A-treated groups. Scale bar = 50 μm. The number of Ki67-positive nuclei per section for each group, and the ROD expressed as a percentage of the value of the TH and DCX immunoreactivity in the dentate gyrus of the vehicle-treated group, are also shown (n = 7 mice per group; **P* < 0.05, versus vehicle-treated group). Data are presented as mean ± SEM. CB1R: CB1 cannabinoid receptor; CB1A: CB1 cannabinoid receptor antagonist; DCX: doublecortin; Pyr: pyridoxine; ROD: relative optical density; SEM: standard error of the mean.

Experimental design 3

Purification and identification of control-PGAM1 and Tat-PGAM1 fusion proteins

Human PGAM1 genes were fused to Tat peptide expression vectors to produce the Tat-PGAM1 fusion proteins. Control-PGAM1 protein, without a Tat domain, was manufactured (Fig. 15A). After the overexpression of the vectors, purified control-PGAM1 and Tat-PGAM1 fusion proteins were obtained by Nib+- → Ni2+-nitrilotriacetic acid sepharose affinity column and PD-10 column chromatography. Western blot analysis revealed polyhistidine bands for control-PGAM1 and Tat-PGAM1 (Fig. 15B).

Confirmation of Tat-PGAM1 delivery into the hippocampus

To confirm the efficient delivery of control-PGAM1 and Tat-PGAM1 fusion proteins into the hippocampus, western blot analysis was conducted. Administration of Tat-PGAM1 significantly increased polyhistidine protein levels in hippocampal homogenates. Administration of Tat peptide or control-PGAM1 resulted in similar polyhistidine protein levels to those in the control group (Fig. 15C).

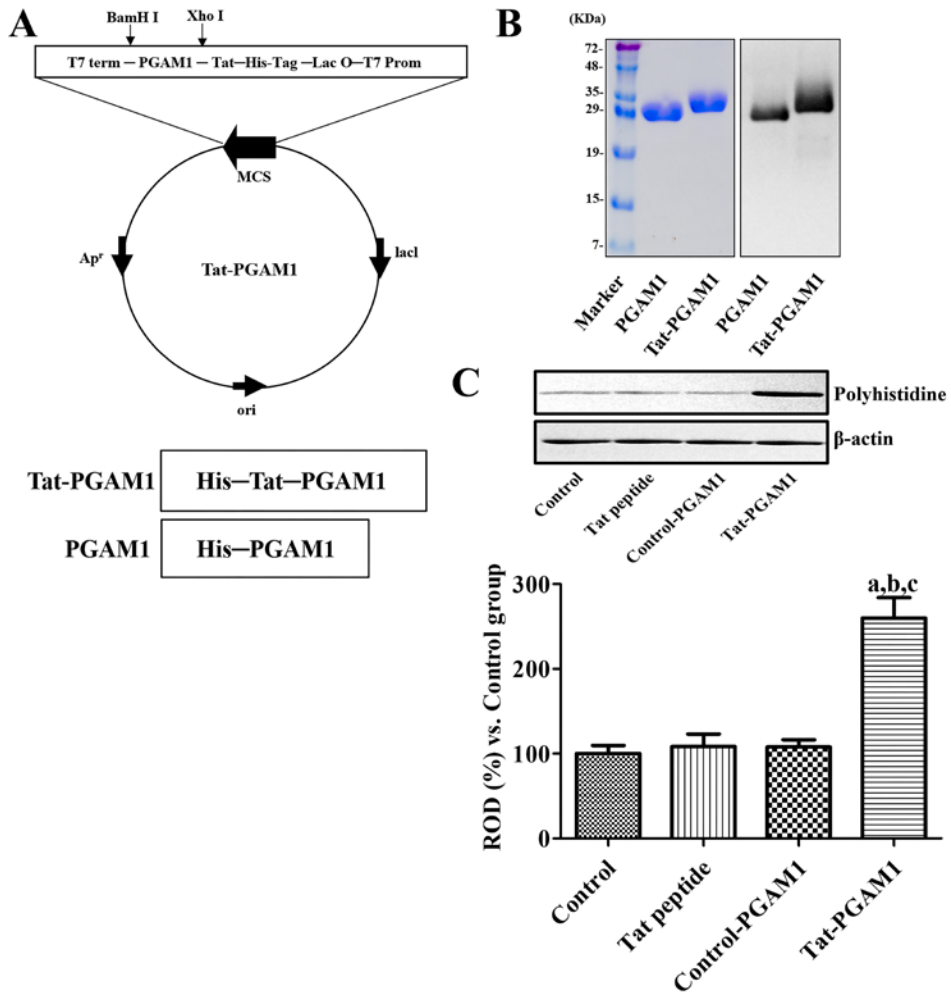

Fig 15. Purification and identification of control-PGAM1 and Tat-PGAM1 fusion proteins and delivery of these proteins into mouse hippocampus. (A) Overview of the control-PGAM1 and Tat-PGAM1 fusion protein. (B) Expression and purification of the control-PGAM1 and Tat-PGAM1 proteins, as assessed by western blot analyses for polyhistidine. (C) Western blot analysis of polyhistidine in hippocampal homogenates of control, Tat peptide-, control-PGAM1-, and Tat-PGAM1-treated groups (n = 5 per group; $^{a}p < 0.05$, versus control group; $^{b}p < 0.05$, versus Tat-peptide-treated group; $^{c}p < 0.05$, versus control-PGAM1-treated group).

Effects of Tat-PGAM1 on novel object recognition memory

Mice spent a similar amount of time exploring the two identical objects in all groups during the training period. However, mice in all groups spent more time exploring the new object than the familiar one during the testing period. Mice in the Tat peptide-treated group spent similar time exploring the new and familiar objects, while the Tat-PGAM1-treated group spent more time exploring the new object than the familiar one. However, no statistically significant difference was detected between the control and Tat peptide-treated groups or between the control and Tat-PGAM1-treated groups. It is notable that the discrimination index was significantly lower in the Tat peptide-treated group and higher in the Tat-PGAM1-treated group than in the control or control-PGAM1-treated groups (Fig 16).

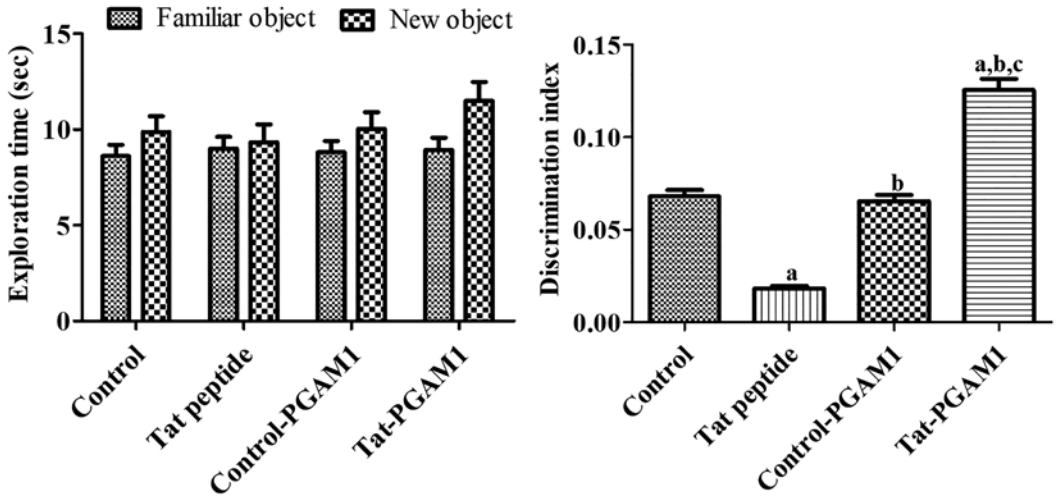

Fig 16. Exploration time (n = 10 per group) and discrimination index (n = 10 per group; $^{a}p < 0.05$, versus control group; $^{b}p < 0.05$, versus Tat-peptide-treated group; $^{c}p < 0.05$, versus control-PGAM1-treated group) of familiar vs. novel objects during testing day of a novel object recognition test in control, Tat peptide-, control-PGAM1-, and Tat-PGAM1-treated mice. Data of the exploration time for each object (same object, where one object was replaced by a new one on the testing day) are presented as a percentage of total exploration time. All data are shown as % exploration time ± SEM.

Effects of Tat-PGAM1 on cell proliferation in the dentate gyrus

In the control group, Ki67-positive proliferating cells were mainly observed in the subgranular zone of the dentate gyrus and the mean number of Ki67-positive nuclei was 12.32 (Fig. 17A and 17E). In the Tat peptide-treated group, few Ki67-positive proliferating cells were found in the dentate gyrus and the number of Ki67-positive nuclei was lower (by 53.41%) than that in the control group (Fig. 17B and 17E). In the control-PGAM1-treated group, Ki67-positive proliferating cells were also mainly observed in the dentate gyrus and the number of Ki67-positive nuclei was 11.06 (Fig. 17C and 17E). In the Tat-PGAM1-treated group, Ki67-positive proliferating cells were observed in the dentate gyrus and the number of Ki67-positive nuclei was significantly higher (by 235.9%) than that in the control group (Fig. 17D and 17E).

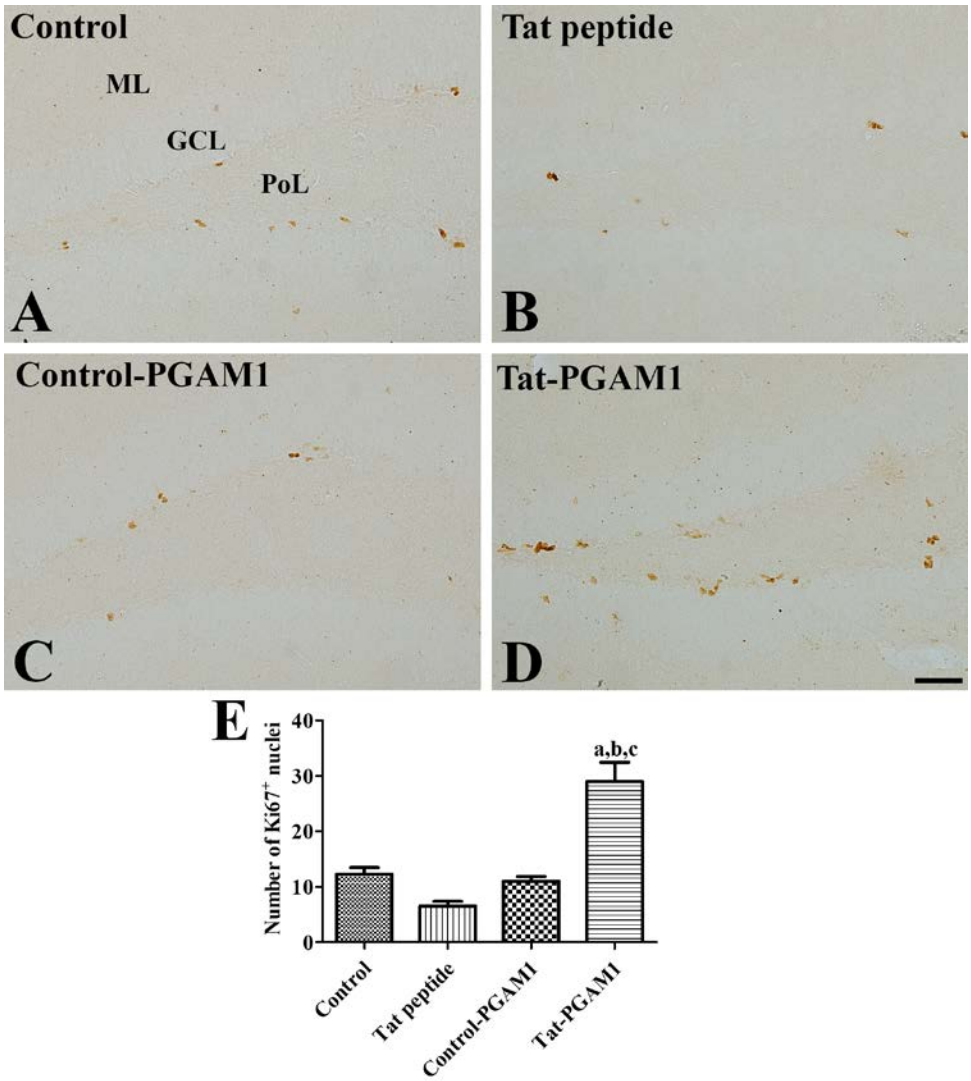
Control
ML
GCL
PoL
A
Tat peptide
B
Control-PGAM1
C
Tat-PGAM1
D
E
Number of Ki67+ nuclei
40
30
20
10
0
a,b,c
Control
Tat peptide
Control-PGAM1
Tat-PGAM1

Fig 17. Immunohistochemistry for Ki67 in the dentate gyrus of (A) control, (B) Tat peptide-, (C) control-PGAM1- and (D) Tat-PGAM1-treated mice. Ki67-positive nuclei are mainly observed in the subgranular zone of the dentate gyrus. Note that Ki67-positive nuclei are few in Tat peptide-treated mice and are most abundant in the dentate gyrus of Tat-PGAM1-treated mice. GCL, granule cell layer; ML, molecular layer; PL, polymorphic layer. Scale bar = 50 μm. (E) The number of Ki67-positive nuclei in the dentate gyrus per section for each group are also shown (n = 5 per group; $^{a}p < 0.05$, versus control group; $^{b}p < 0.05$, versus Tat-peptide-treated group; $^{c}p < 0.05$, versus control-PGAM1-treated group). Data are presented as mean ± SEM.

Effects of Tat-PGAM1 on neuroblast differentiation in the dentate gyrus

In the control group, DCX-immunoreactive differentiated neuroblasts were detected in the dentate gyrus. In this group, DCX immunoreactivity was found in the cytoplasm and dendrites, which extended into the molecular layer of dentate gyrus (Fig. 18A). In the Tat peptide-treated group, DCX immunoreactive differentiated neuroblasts were few and their dendrites were poorly developed in the dentate gyrus. DCX immunoreactivity was significantly lower, by 28.26%, than that in the control group (Fig. 18B and 18E). In the control-PGAM1-treated group, DCX-immunoreactive differentiated neuroblasts were observed to have a distribution pattern similar to that in the control group, and DCX immunoreactivity was slightly higher than that in the control group (Fig. 18C and 18E). The DCX-immunoreactive differentiated neuroblasts were more abundant in the dentate gyrus in the Tat-PGAM1-treated group than in this region in the control or control-PGAM1-treated group. Further, in the Tat-PGAM1-treated group, DCX immunoreactivity was significantly higher, by 173.56%, than that in the control group (Fig. 18D and 18E).

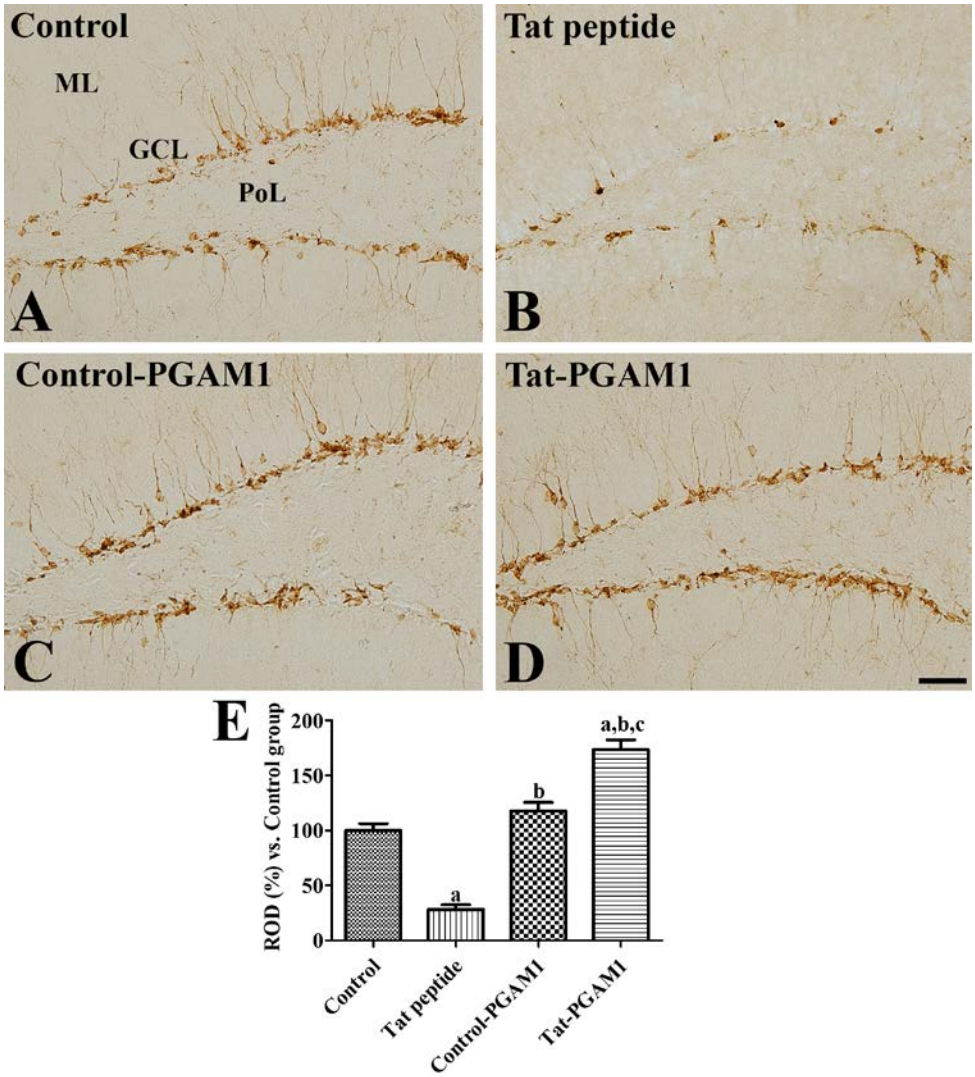
Control
ML
GCL
PoL
A
Tat peptide
B
Control-PGAM1
C
Tat-PGAM1
D
E
ROD (%) vs. Control group
200
150
100
50
0
a
b
a,b,c
Control
Tat peptide
Control-PGAM1
Tat-PGAM1

Fig 18. Immunohistochemistry for DCX in the dentate gyrus of (A) control, (B) Tat peptide-, (C) control-PGAM1- and (D) Tat-PGAM1-treated mice. DCX-immunoreactive neuroblasts have cytoplasm located in the subgranular zone and have dendrites extending into the molecular layer (ML) of the dentate gyrus. DCX-immunoreactive neuroblasts and their dendrites are poorly detected in the dentate gyrus of Tat peptide-treated mice, but are most abundant in the dentate gyrus of Tat-PGAM1-treated mice. GCL, granule cell layer; PL, polymorphic layer. Scale bar = 50 μm. (E) The relative optical densities (RODs) expressed as a percentage of the value representing the DCX immunoreactivity in the dentate gyrus of the control group are also shown (n = 5 per group; $^{a}p < 0.05$, versus control group; $^{b}p < 0.05$, versus Tat-peptide-treated group; $^{c}p < 0.05$, versus control-PGAM1-treated group). Data are presented as mean ± SEM.

Effects of Tat-PGAM1 on the phosphorylation of CREB in the dentate gyrus

In the control group, pCREB-positive nuclei were mainly observed in the subgranular zone of the dentate gyrus and the mean number of pCREB-positive nuclei was 46.70 (Fig. 19A and 19E). In the Tat peptide-treated group, few pCREB-positive nuclei were found in the dentate gyrus and the number of pCREB-positive nuclei was lower, by 54.05%, than that in the control group (Fig. 19B and 19E). pCREB positive nuclei were detected in the dentate gyrus both in the control and control-PGAM1-treated groups although the number of pCREB-positive nuclei was slightly higher than that in the control group (Fig. 19C and 19E). pCREB-positive nuclei were more abundantly observed in the dentate gyrus in the Tat-PGAM1-treated group than in this region in the control or control-PGAM1-treated group. Moreover, in the Tat-PGAM1-treated group, the number of pCREB-positive nuclei was significantly higher, by 154.7%, than in the control group (Fig. 19D and 19E).

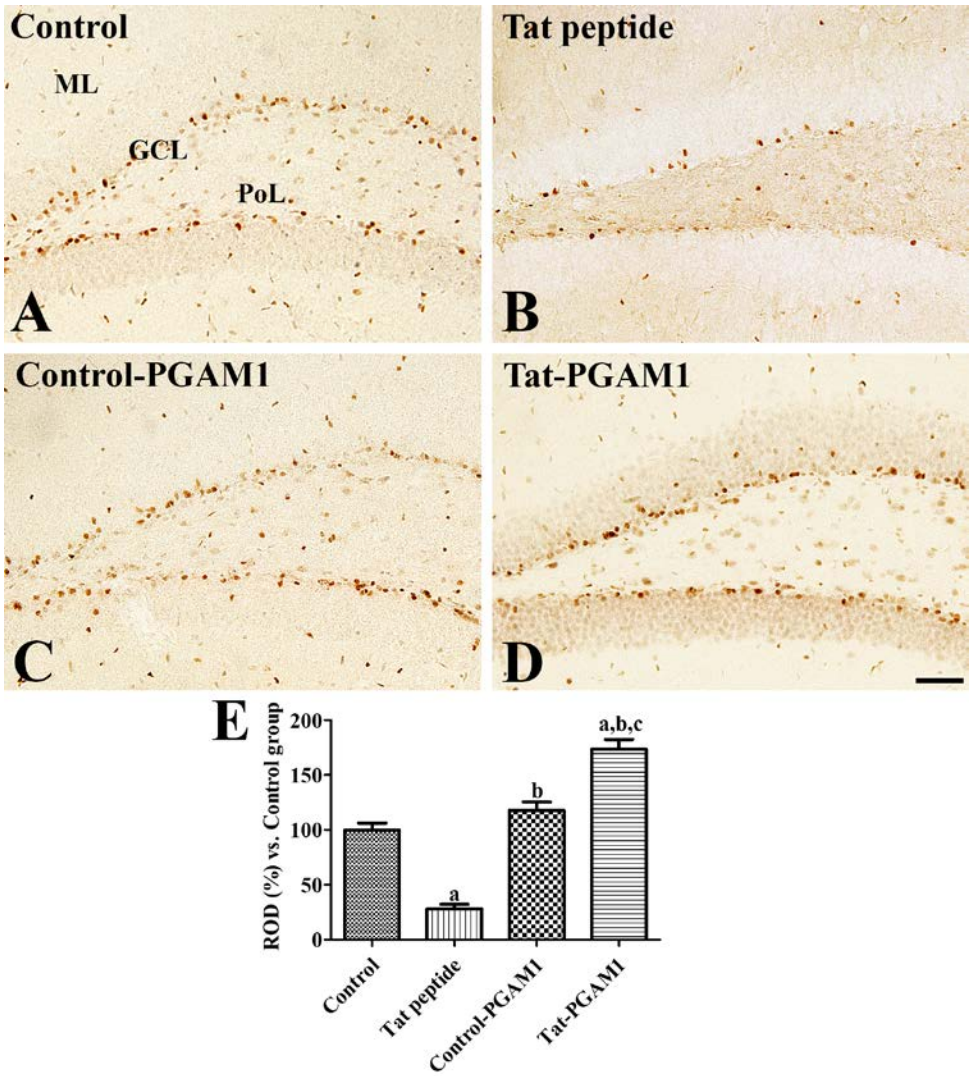
Control
ML
GCL
PoL
A
Tat peptide
B
Control-PGAM1
C
Tat-PGAM1
D
E
ROD (%) vs. Control group
200
150
100
50
0
a
b
a,b,c
Control
Tat peptide
Control-PGAM1
Tat-PGAM1

Fig 19. Immunohistochemistry for pCREB in the dentate gyrus of (A) control, (B) Tat peptide-, (C) control-PGAM1- and (D) Tat-PGAM1-treated mice. pCREB-positive nuclei are mainly found in the subgranular zone of the dentate gyrus. Note that pCREB-positive nuclei are few in the dentate gyrus of Tat peptide-treated mice, while pCREB-positive nuclei are strong and most abundant in the dentate gyrus of Tat-PGAM1-treated mice. GCL, granule cell layer; ML, molecular layer; PL, polymorphic layer. Scale bar = 50 μm. (E) The number of pCREB-positive nuclei per section for each group are also shown (n = 5 per group; $^{a}p < 0.05$, versus control group; $^{b}p < 0.05$, versus Tat-peptide-treated group; $^{c}p < 0.05$, versus control-PGAM1-treated group). Data are presented as mean ± SEM.

Discussion

Recently, monoaminergic neurotransmitters such as serotonin, norepinephrine, and dopamine have emerged as critical players in the modulation of mood and emotion, as well as in the control of motor, perceptual, and other cognitive functions (Feldman and Quenzer, 1984). Pyridoxine deficiency in mothers result in behavioral abnormalities and intellectual deficits in the progeny (Krishna and Ramakrishna, 2004) and alters the N-methyl-D-aspartate receptor function, which plays an important role in learning and memory (Guilarte, 1993). In contrast, supplementation of vitamin B_6 to elderly men showed positive effects on long-term memory (Deijen et al., 1992). In addition, we showed the positive effects of pyridoxine on hippocampal neurogenesis in both the young-adult and aged mice (Yoo et al., 2011; Yoo et al., 2012a). Hippocampal neurogenesis is an important factor for spatial and object recognition memory (Jessberger et al., 2009). In the present study, we investigated the effects of pyridoxine, a cofactor involved in the synthesis of these monoamines, on novel object recognition memory, and on proteomics of hippocampal homogenates. Pyridoxine administered animals showed significantly better novel object recognition memory compared to vehicle-treated animals.

Previous studies showed a correlation between blood levels of vitamin B and cognitive functions (Goodwin et al., 1983; La Rue et al., 1997). In addition, high concentrations of vitamin B_6 have been associated with high performance in memory tests (e.g., backward digit span test) in humans (Riggs et al., 1996). Conversely, several studies have reported an inverse relationship between plasma pyridoxine concentration and age (Bates et al., 1999; Joosten et al., 1993; Pannemans et al., 1994; Rose et al., 1976). In an animal study, administration of pyridoxine with insulin and *Aegle marmelos* leaf extract improved streptozotocin-induced decrease in memory function, as assessed through elevated plus maze test (Abraham et al., 2010).

In the present study, we focused on the levels of 5-HT and 5-HIAA in the hippocampal homogenates in order to elucidate the changes in serotonin turnover, based on several electrophysiological studies which showed that the prefrontal cortex and raphe nucleus exhibit bidirectional projections (Amargos-Bosch et al., 2004; Celada et al., 2001; Puig et al., 2005; Puig et al., 2003). The ratio of 5-HIAA/5-HT was significantly lower in the pyridoxine-treated group than in the control group, suggesting that pyridoxine may enhance the effects of serotonin in the hippocampus similar to antidepressants such as fluoxetine (Stenfors and Ross, 2002). This finding is consistent with those of a previous study, which revealed that increase in extracellular 5-HT improves memory performance, while reduced levels are associated with impaired spatial memory (Kuypers and Ramaekers, 2005; Lesch et al., 1996). Vortioxetine, a serotonin reuptake inhibitor, increases novel object recognition memory, which can be prevented by the administration of SR57227, a 5-HT3 receptor antagonists (Betry et al., 2015). In addition, administration of pyridoxine along with insulin ameliorates diabetes-induced turnover of serotonin into 5-HIAA in the cerebral cortex (Abraham et al., 2010). Several lines of evidence suggest that chronic stimulation of the ventromedial prefrontal cortex with pyridoxine enhances short- and long-term memory during novel object recognition tests and Morris water-maze tasks (Liu et al., 2015) and significantly increases cell proliferation as well as neurogenesis-associated gene expression (Liu et al., 2015). In the present study, we observed changes in TH immunoreactivity in the hippocampus and the TH immunoreactive fibers project from the substantia nigra to the hippocampal dentate gyrus (Hoglinger et al., 2014; Hoglinger et al., 2004; Lisman and Grace, 2005; Mu et al., 2011; Swanson, 1982). Further, we observed that, pyridoxine treatment significantly increased TH immunoreactivity in the dentate gyrus. This result is supported by a previous study which showed that dopaminergic lesions significantly decrease neurogenesis in the hippocampus (Schlachetzki et al., 2016). In contrast, treatment with

levodopa reversed the reduction in hippocampal neurogenesis caused by bilateral treatment of the substantia nigra with 6-hydroxydopa (Chiu et al., 2015). Administration of the non-ergoline D2/D3-receptor agonist PPX significantly increased adult neurogenesis in the hippocampal dentate gyrus of naïve mice (Salvi et al., 2016).

In the present study, we identified several differentially expressed proteins in the pyridoxine-treated hippocampus using DIGE coupled with MALDI-TOF MS. We observed three protein spots showing at least 1.5-fold change, and subsequently identified these spots as CRIP1a and PGAM1. Further, we validated the expression of these genes by examining mRNA levels. A significant decrease in CRIP1a mRNA and protein levels was observed in hippocampal homogenates in the pyridoxine-treated group. In addition, CRIP1a immunoreactivity was decreased in the stratum pyramidale of the hippocampal CA1 region and in the granule cell layer of the dentate gyrus. There have been reports that CB1R is highly expressed in the stratum pyramidale of the CA1 region and in the granule cell layer of the dentate gyrus (Xu et al., 2010). The patterns of expression in these regions may be indicative of a great association between CB1R and CRIP1a in the hippocampus. A previous study showed that CRIP1a specifically interacts with CB1Rs (Niehaus et al., 2007). CB1R and CRIP1a are co-expressed in major fields of the hippocampal formation including GABAergic interneurons and glutamatergic pyramidal neurons, and regulate embryonic cell fate in the developing brain as well as neurogenesis in the adult brain (Aguado et al., 2005; Diaz-Alonso et al., 2012; Goncalves et al., 2008). In addition, CB1 regulates memory/cognition, motor activity, motivation, anxiety, appetite, and energy balance (Howlett et al., 2002). Overexpression of CRIP1a inhibits constitutive CB1R activity as well as agonist-stimulated CB1R signaling in cultured autaptic hippocampal neurons (Blume et al., 2016). The results of the present study, in the light of the aforementioned findings, indicate that decrease in CRIP1a induced by pyridoxine treatment promotes CB1R function and may enhance

neurogenesis.

In the present study, we observed an increase in PGAM1 mRNA level in the hippocampal homogenates of the pyridoxine-treated group. PGAM1 is an enzyme that catalyzes the interconversion of 3-phosphoglycerate and 2-phosphoglycerate during glycolysis. Previous studies have reported that this enzyme is upregulated in several human cancers such as colorectal cancer (Usuba et al., 2001), lung cancer (Li et al., 2006), breast carcinoma (Durany et al., 2000), esophagus squamous cell carcinoma (Fang et al., 2004), breast cancer, prostate cancer (Betry et al., 2015), oral squamous cellular carcinoma (Turhani et al., 2006), and glioma (Gao et al., 2013; Jain et al., 2015) and therefore, may promote cancer cell proliferation. Interference of PGAM1 with PGAM1 shRNA inhibits proliferation and increases apoptosis in T24 and EJ cell lines (Peng et al., 2016), and increases survival of mice with glioblastoma (Sanzey et al., 2015). In the present study, the increase in PGAM1 level facilitated glycolysis, thus, increasing the energy supply in the hippocampus. In neurodegenerative conditions such as Alzheimer's disease, PGAM1 is significantly oxidized which reduces its enzymatic activities (Boyd-Kimball et al., 2005; Sultana et al., 2006), as evidenced by 70% decrease in PGAM1 protein levels relative to controls (Sultana et al., 2007).

In the present study, we observed that administration of CRIP1a siRNA significantly reduced the CRIP1a protein expression 7 weeks after the treatment, and significantly improved the discrimination index as measured by the novel object recognition test. It also increased cell proliferation and neuroblast differentiation in the dentate gyrus as assessed by Ki67 and DCX immunohistochemistry. These results suggest that pyridoxine significantly improves novel object recognition and hippocampal neurogenesis by reducing CRIP1a expression in the hippocampus.

In the present study, we investigated the direct effects of CB1R signaling on hippocampal

functions, including novel object recognition memory, 5-HT turnover, TH immunoreactivity, cell proliferation, and neuroblast differentiation. Administration of rimonabant, a well-known CB1R antagonist intended for the treatment of obesity (Colombo et al., 1998), significantly decreased novel object recognition memory, TH immunoreactivity, cell proliferation, and neuroblast differentiation in the dentate gyrus. There has been conflicting evidence regarding the effects and treatment duration of rimonabant on the memory functions in animals. CB1R knockout mice showed enhanced spontaneous alternation performance and preference toward the novel object in the arm maze performance (Basavarajappa and Subbanna, 2014). In contrast, a single dose of rimonabant impairs positive affective memory in healthy volunteers (Horder et al., 2009). Another study showed that rimonabant dose-dependently inhibits the memory recalls in the passive avoidance task in chicks (Adam et al., 2008). In addition, administration of 1 mg/kg SR141716, a CB1 receptor antagonist to rats has no effect on cognition (Hasanein and Teimuri Far, 2015). In the present study, we observed that the administration of rimonabant significantly reduced cognitive function and TH immunoreactivity in the hippocampus. This result is consistent with a previous study, which showed that the male CB1 receptor knockout mice had greater anxiety-like behavior compared with sex-matched wild-type controls as measured by the percent of open-arm entries in an elevated plus-maze test (Bowers and Ressler, 2016).

In the present study, we observed that rimonabant significantly decreased cell proliferation and neuroblast differentiation in the dentate gyrus. This result is consistent with those of a previous study, which showed that the administration of rimonabant significantly decreased the number of DCX-immunoreactive neuroblasts located in the subgranular zone of the dentate gyrus (Lee et al., 2009). In addition, CB1R activation increased neurogenesis in the in vitro culture system (Xapelli et al., 2013), while knockout of CB1R signaling results in defective neurogenesis in mice (Jin et al., 2004).

In the present study, pyridoxine treatment significantly increased novel object recognition memory and slightly, but not significantly, reversed the rimonabant-induced reduction in 5-HT and 5-HIAA levels, TH immunoreactivity, cell proliferation, and neuroblast differentiation in the dentate gyrus. This result suggests that pyridoxine increases hippocampal neurogenesis by modulating both CB1R signaling and CRIP1a protein levels in the hippocampus.

In the present study, we investigated the role of PGAM1 in cell proliferation and neuroblast differentiation in the mouse dentate gyrus. Our data suggest that cancer and hippocampal neurogenesis share similar microenvironment and metabolic pathways. We examined the effects of PGAM1 on novel object recognition memory, cell proliferation, and neuroblast differentiation in the dentate gyrus.

To facilitate the delivery of PGAM1 into neurons, we generated a Tat-PGAM1 fusion protein attached to a polyhistidine tag and we confirmed the successful delivery of the Tat-PGAM1 fusion protein in the hippocampus by western blot using anti-polyhistidine antibody. Administration of Tat-PGAM1 significantly increased the polyhistidine levels in the hippocampus, while control-PGAM1 treatment did not show any significant change in the levels of polyhistidine. This result indicates that control-PGAM1 was not able to cross the blood-brain barrier or cell membrane, while Tat-PGAM1 fusion protein effectively crossed the blood-brain barrier and cell membrane. Tat-fusion protein can be utilized in research on neurological disorders including Alzheimer’s disease and cerebral ischemia (Buccarello and Borsello, 2017; Tu et al., 2015; Kim et al., 2015).

It has been reported that during HIV infection, the virus associated Tat protein is one of the causative agents in HIV-associated neurocognitive disorders (Gannon et al., 2011; Irish et al., 2009). In addition, Tat peptide has been linked to impaired neurogenesis and cognitive deficits (Ferrell and Giunta, 2014; Fan et al., 2016). In the present study, we

also observed a significant reduction in novel object recognition, as well as cell proliferation and neuroblast differentiation in the dentate gyrus of Tat peptide-treated mice. Intrahippocampal administration of Tat protein in rats resulted in behavioral deficits in the Morris water maze and novel object recognition tests (Harricharan et al., 2015). Tat-expressing mouse brain showed a significant reduction in the numbers of neural stem cells and neuroblasts and its differentiation into mature neurons. In addition, Tat-containing conditioned media impaired proliferation, migration, and differentiation of neural precursor cells through Notch signaling (Fan et al., 2016). Administration of Tat-PGAM1 to mice increased the time spent exploring the new object, although statistical significance was not detected. However, the DI was significantly higher in the Tat-PGAM1-treated group than in the control or control-PGAM1-treated groups. This result suggests that administration of Tat-PGAM1 improves novel object recognition memory. To elucidate the effects of Tat-PGAM1 on cell proliferation and neuroblast differentiation in the dentate gyrus, we conducted immunohistochemical staining for Ki67 and DCX, respectively. Administration of Tat-PGAM1, but not control-PGAM1, significantly increased the number of proliferating cells and differentiated neuroblasts in the dentate gyrus. This result suggests that PGAM1 facilitates glycolysis in order to promote cell proliferation and neuroblast differentiation in the dentate gyrus. This result is supported by previous studies that showed that targeting PGAM1 with siRNA or a small molecule inhibitor, PGMI-004A, induced cell death by up-regulating the apoptotic pathway and down-regulating the anti-apoptotic pathway (Xu et al., 2016), attenuated cancer cell proliferation (Ren et al., 2010; Hitosugi et al., 2012), and reduced cell motility (Zhang et al., 2017). However, a recent study demonstrated that knockdown of PGAM1 partially reduced glycolysis (Zhang et al., 2017). Another possibility is that PGAM1 modulates actin filament assembly, cell motility, and cell migration, as shown in cancer cells, through direct interaction with α-smooth muscle actin ACTA2, independent

of its metabolic activity (Zhang et al., 2017).

CREB is one of the most important transcription factors mediating neural plasticity in the mammalian brain. Depletion of CREB results in impaired axonal growth and projections (Lonze et al., 2002), while activation of CREB in cortical neurons induces dendritic growth and arborization (Redmond et al., 2002). In addition, CREB regulates the expression of glucose transporter 3 (GLUT3) and pharmacological inhibition of glycolysis impairs neurite growth (Segarra-Mondejar et al., 2018). In previous studies, we demonstrated that GLUT3 and glucose metabolism are closely related to hippocampal neurogenesis in the gerbil hippocampus after transient forebrain ischemia (Yoo et al., 2016) as well as postnatal development in the mouse hippocampus (Jung et al., 2016). Furthermore, we demonstrated that administration of pyridoxine significantly increased the number of pCREB-immunoreactive nuclei in the high-fat diet-fed mice (Yoo et al., 2012). In the present study, we have demonstrated that administration of Tat-PGAM1 significantly increases the phosphorylation of CREB in the dentate gyrus. Collectively, these results suggest that PGAM1 increases phosphorylation of CREB and facilitates synaptic plasticity, cell proliferation, and neuroblast differentiation, as well as glucose metabolism, in the hippocampus. To confirm the role of PGAM1 on hippocampal neurogenesis and cognitive functions, a knockout studies for PGAM1 needs to be planned as there are currently no knockout mice for Pgam1.

Conflicts of interest

This study was published in the BBA-General Subjects (Biochimica et Biophysica Acta-General Subjects) and neurochemical research in 2017 and 2019, respectively. (Jung et al., 2017; Jung et al., 2019)

References

Abraham, P.M., Kuruvilla, K.P., Mathew, J., Malat, A., Joy, S., Paulose, C.S., 2010. Alterations in hippocampal serotonergic and INSR function in streptozotocin induced diabetic rats exposed to stress: neuroprotective role of pyridoxine and Aegle marmelose. Journal of biomedical science 17, 78.

Adam, A.S., Wenger, T., Csillag, A., 2008. The cannabinoid CB1 receptor antagonist rimonabant dose-dependently inhibits memory recall in the passive avoidance task in domestic chicks (Gallus domesticus). Brain research bulletin 76, 272-274.

Aguado, T., Monory, K., Palazuelos, J., Stella, N., Cravatt, B., Lutz, B., Marsicano, G., Kokaia, Z., Guzman, M., Galve-Roperh, I., 2005. The endocannabinoid system drives neural progenitor proliferation. FASEB journal : official publication of the Federation of American Societies for Experimental Biology 19, 1704-1706.

Altman, J., Das, G.D., 1965. Autoradiographic and histological evidence of postnatal hippocampal neurogenesis in rats. The Journal of comparative neurology 124, 319-335.

Amargos-Bosch, M., Bortolozzi, A., Puig, M.V., Serrats, J., Adell, A., Celada, P., Toth, M., Mengod, G., Artigas, F., 2004. Co-expression and in vivo interaction of serotonin1A and serotonin2A receptors in pyramidal neurons of prefrontal cortex. Cerebral cortex (New York, N.Y. : 1991) 14, 281-299.

Balu, D.T., Lucki, I., 2009. Adult hippocampal neurogenesis: Regulation, functional implications, and contribution to disease pathology. Neuroscience & Biobehavioral

Reviews 33, 232-252.

Banasr, M., Hery, M., Printemps, R., Daszuta, A., 2004. Serotonin-induced increases in adult cell proliferation and neurogenesis are mediated through different and common 5-HT receptor subtypes in the dentate gyrus and the subventricular zone. Neuropsychopharmacology : official publication of the American College of Neuropsychopharmacology 29, 450-460.

Basavarajappa, B.S., Subbanna, S., 2014. CB1 receptor-mediated signaling underlies the hippocampal synaptic, learning, and memory deficits following treatment with JWH-081, a new component of spice/K2 preparations. Hippocampus 24, 178-188.

Bates, C.J., Pentieva, K.D., Prentice, A., Mansoor, M.A., Finch, S., 1999. Plasma pyridoxal phosphate and pyridoxic acid and their relationship to plasma homocysteine in a representative sample of British men and women aged 65 years and over. The British journal of nutrition 81, 191-201.

Beckervordersandforth, R., Zhang, C.L., Lie, D.C., 2015. Transcription-Factor-Dependent Control of Adult Hippocampal Neurogenesis. Cold Spring Harbor perspectives in biology 7, a018879.

Betry, C., Etievant, A., Pehrson, A., Sanchez, C., Haddjeri, N., 2015. Effect of the multimodal acting antidepressant vortioxetine on rat hippocampal plasticity and recognition memory. Progress in neuro-psychopharmacology & biological psychiatry 58, 38-46.

Blume, L.C., Leone-Kabler, S., Luessen, D.J., Marrs, G.S., Lyons, E., Bass, C.E., Chen, R., Selley, D.E., Howlett, A.C., 2016. Cannabinoid receptor interacting protein suppresses agonist-driven CB1 receptor internalization and regulates receptor replenishment in an agonist-biased manner. Journal of neurochemistry 139, 396-407.

Bowers, M.E., Ressler, K.J., 2016. Sex-dependence of anxiety-like behavior in cannabinoid receptor 1 (Cnr1) knockout mice. Behavioural brain research 300, 65-69.

Boyd-Kimball, D., Sultana, R., Poon, H.F., Lynn, B.C., Casamenti, F., Pepeu, G., Klein, J.B., Butterfield, D.A., 2005. Proteomic identification of proteins specifically oxidized by intracerebral injection of amyloid beta-peptide (1-42) into rat brain: implications for Alzheimer's disease. Neuroscience 132, 313-324.

Cameron, H.A., Mckay, R.D., 2001. Adult neurogenesis produces a large pool of new granule cells in the dentate gyrus. Journal of Comparative Neurology 435, 406-417.

Castilla-Ortega, E., Pedraza, C., Estivill-Torrus, G., Santin, L.J., 2011. When is adult hippocampal neurogenesis necessary for learning? evidence from animal research. Reviews in the neurosciences 22, 267-283.

Celada, P., Puig, M.V., Casanovas, J.M., Guillazo, G., Artigas, F., 2001. Control of dorsal raphe serotonergic neurons by the medial prefrontal cortex: Involvement of serotonin-1A, GABA(A), and glutamate receptors. The Journal of neuroscience : the official journal of the Society for Neuroscience 21, 9917-9929.

Chiu, W.H., Depboylu, C., Hermanns, G., Maurer, L., Windolph, A., Oertel, W.H., Ries, V., Hoglinger, G.U., 2015. Long-term treatment with L-DOPA or pramipexole affects

adult neurogenesis and corresponding non-motor behavior in a mouse model of Parkinson's disease. Neuropharmacology 95, 367-376.

Coburn, S.P., 2015. Vitamin B-6 Metabolism and Interactions with TNAP. Sub-cellular biochemistry 76, 207-238.

Colombo, G., Agabio, R., Diaz, G., Lobina, C., Reali, R., Gessa, G.L., 1998. Appetite suppression and weight loss after the cannabinoid antagonist SR 141716. Life sciences 63, Pl113-117.

Deijen, J.B., van der Beek, E.J., Orlebeke, J.F., van den Berg, H., 1992. Vitamin B-6 supplementation in elderly men: effects on mood, memory, performance and mental effort. Psychopharmacology 109, 489-496.

Deng, W., Aimone, J.B., Gage, F.H., 2010. New neurons and new memories: how does adult hippocampal neurogenesis affect learning and memory? Nature reviews. Neuroscience 11, 339-350.

Edmondson, D., Mattevi, A., Binda, C., Li, M., Hubalek, F., 2004. Structure and mechanism of monoamine oxidase. Current medicinal chemistry 11, 1983-1993.

Diaz-Alonso, J., Guzman, M., Galve-Roperh, I., 2012. Endocannabinoids via CB(1) receptors act as neurogenic niche cues during cortical development. Philosophical transactions of the Royal Society of London. Series B, Biological sciences 367, 3229-3241.

Edmondson, D.E., Mattevi, A., Binda, C., Li, M., Hubalek, F., 2004. Structure and

mechanism of monoamine oxidase. Current medicinal chemistry 11, 1983-1993.

Eichenbaum, H., 2017. The role of the hippocampus in navigation is memory. Journal of neurophysiology 117, 1785-1796.

Feldman, R.S., Quenzer, L.F., 1984. Fundamentals of neuropsychopharmacology. Sinauer Associates Sunderland, MA.

Franklin, K.B.J., Paxinos, G., 1997. The mouse brain in stereotaxic coordinates. Academic press, san diego.

Goncalves, J.T., Schafer, S.T., Gage, F.H., 2016. Adult Neurogenesis in the Hippocampus: From Stem Cells to Behavior. Cell 167, 897-914.

Goncalves, M.B., Suetterlin, P., Yip, P., Molina-Holgado, F., Walker, D.J., Oudin, M.J., Zentar, M.P., Pollard, S., Yanez-Munoz, R.J., Williams, G., Walsh, F.S., Pangalos, M.N., Doherty, P., 2008. A diacylglycerol lipase-CB2 cannabinoid pathway regulates adult subventricular zone neurogenesis in an age-dependent manner. Molecular and cellular neurosciences 38, 526-536.

Goodwin, J.S., Goodwin, J.M., Garry, P.J., 1983. Association between nutritional status and cognitive functioning in a healthy elderly population. Jama 249, 2917-2921.

Gordon, N., Goelman, G., 2016. Understanding alterations in serotonin connectivity in a rat model of depression within the monoamine-deficiency and the hippocampal-neurogenesis frameworks. Behavioural brain research 296, 141-148.

Gould, E., Tanapat, P., Hastings, N.B., Shors, T.J., 1999. Neurogenesis in adulthood: a possible role in learning. Trends in cognitive sciences 3, 186-192.

Guilarte, T.R., 1993. Vitamin B6 and cognitive development: recent research findings from human and animal studies. Nutrition reviews 51, 193-198.

Hasanein, P., Teimuri Far, M., 2015. Effects of URB597 as an inhibitor of fatty acid amide hydrolase on WIN55, 212-2-induced learning and memory deficits in rats. Pharmacology, biochemistry, and behavior 131, 130-135.

Hoglinger, G.U., Arias-Carrion, O., Ipach, B., Oertel, W.H., 2014. Origin of the dopaminergic innervation of adult neurogenic areas. The Journal of comparative neurology 522, 2336-2348.

Hoglinger, G.U., Rizk, P., Muriel, M.P., Duyckaerts, C., Oertel, W.H., Caille, I., Hirsch, E.C., 2004. Dopamine depletion impairs precursor cell proliferation in Parkinson disease. Nature neuroscience 7, 726-735.

Horder, J., Cowen, P.J., Di Simplicio, M., Browning, M., Harmer, C.J., 2009. Acute administration of the cannabinoid CB1 antagonist rimonabant impairs positive affective memory in healthy volunteers. Psychopharmacology 205, 85-91.

Howlett, A.C., Barth, F., Bonner, T.I., Cabral, G., Casellas, P., Devane, W.A., Felder, C.C., Herkenham, M., Mackie, K., Martin, B.R., Mechoulam, R., Pertwee, R.G., 2002. International Union of Pharmacology. XXVII. Classification of cannabinoid receptors. Pharmacological reviews 54, 161-202.

Jensen, P.K., Pasa-Tolic, L., Anderson, G.A., Horner, J.A., Lipton, M.S., Bruce, J.E., Smith, R.D., 1999. Probing proteomes using capillary isoelectric focusing-electrospray

ionization Fourier transform ion cyclotron resonance mass spectrometry. Analytical chemistry 71, 2076-2084.

Jessberger, S., Clark, R.E., Broadbent, N.J., Clemenson, G.D., Jr., Consiglio, A., Lie, D.C., Squire, L.R., Gage, F.H., 2009. Dentate gyrus-specific knockdown of adult neurogenesis impairs spatial and object recognition memory in adult rats. Learning & memory (Cold Spring Harbor, N.Y.) 16, 147-154.

Jin, K., Xie, L., Kim, S.H., Parmentier-Batteur, S., Sun, Y., Mao, X.O., Childs, J., Greenberg, D.A., 2004. Defective adult neurogenesis in CB1 cannabinoid receptor knockout mice. Molecular pharmacology 66, 204-208.

Jin, X., 2016. The role of neurogenesis during development and in the adult brain. The European journal of neuroscience 44, 2291-2299.

Joosten, E., van den Berg, A., Riezler, R., Naurath, H.J., Lindenbaum, J., Stabler, S.P., Allen, R.H., 1993. Metabolic evidence that deficiencies of vitamin B-12 (cobalamin), folate, and vitamin B-6 occur commonly in elderly people. The American journal of clinical nutrition 58, 468-476.

Jung, H.Y., Kim, D.W., Nam, S.M., Kim, J.W., Chung, J.Y., Won, M.H., Seong, J.K., Yoon, Y.S., Yoo, D.Y., Hwang, I.K., 2017. Pyridoxine improves hippocampal cognitive function via increases of serotonin turnover and tyrosine hydroxylase, and its association with CB1 cannabinoid receptor-interacting protein and the CB1 cannabinoid receptor pathway. Biochimica et biophysica acta. General subjects 1861, 3142-3153.

Jung, H.Y., Kwon, H.J., Kim, W., Nam, S.M., Kim, J.W., Hahn, K.R., Yoo, D.Y., Won, M.H., Yoon, Y.S., Kim, D.W., Hwang, I.K., 2019. Phosphoglycerate Mutase 1 Promotes Cell Proliferation and Neuroblast Differentiation in the Dentate Gyrus by Facilitating the Phosphorylation of cAMP Response Element-Binding Protein. Neurochemical research 44, 323-332.

Jung, H.Y., Yoo, D.Y., Nam, S.M., Kim, J.W., Choi, J.H., Yoo, M., Lee, S., Yoon, Y.S., Hwang, I.K., 2015. Valerenic Acid Protects Against Physical and Psychological Stress by Reducing the Turnover of Serotonin and Norepinephrine in Mouse Hippocampus-Amygdala Region. Journal of medicinal food 18, 1333-1339.

Kempermann, G., Song, H., Gage, F.H., 2015. Neurogenesis in the Adult Hippocampus. Cold Spring Harbor perspectives in biology 7, a018812.

Krishna, A., Ramakrishna, T., 2004. Effect of pyridoxine deficiency on the structural and functional development of hippocampus. Indian journal of physiology and pharmacology 48, 304-310.

Kuypers, K.P., Ramaekers, J.G., 2005. Transient memory impairment after acute dose of 75mg 3.4-Methylene-dioxymethamphetamine. Journal of psychopharmacology (Oxford, England) 19, 633-639.

La Rue, A., Koehler, K.M., Wayne, S.J., Chiulli, S.J., Haaland, K.Y., Garry, P.J., 1997. Nutritional status and cognitive functioning in a normally aging sample: a 6-y reassessment. The American journal of clinical nutrition 65, 20-29.

Lee, S., Kim, D.H., Yoon, S.H., Ryu, J.H., 2009. Sub-chronic administration of rimonabant causes loss of antidepressive activity and decreases doublecortin immunoreactivity in the mouse hippocampus. Neuroscience letters 467, 111-116.

Lesch, K.P., Bengel, D., Heils, A., Sabol, S.Z., Greenberg, B.D., Petri, S., Benjamin, J., Muller, C.R., Hamer, D.H., Murphy, D.L., 1996. Association of anxiety-related traits with a polymorphism in the serotonin transporter gene regulatory region. Science (New York, N.Y.) 274, 1527-1531.

Lisman, J.E., Grace, A.A., 2005. The hippocampal-VTA loop: controlling the entry of information into long-term memory. Neuron 46, 703-713.

Liu, A., Jain, N., Vyas, A., Lim, L.W., 2015. Ventromedial prefrontal cortex stimulation enhances memory and hippocampal neurogenesis in the middle-aged rats. eLife 4.

Malouf, R., Grimley Evans, J., 2003. The effect of vitamin B6 on cognition. The Cochrane database of systematic reviews, Cd004393.

Mu, Y., Gage, F.H., 2011. Adult hippocampal neurogenesis and its role in Alzheimer's disease. Molecular neurodegeneration 6, 85.

Mu, Y., Zhao, C., Gage, F.H., 2011. Dopaminergic modulation of cortical inputs during maturation of adult-born dentate granule cells. The Journal of neuroscience : the official journal of the Society for Neuroscience 31, 4113-4123.

Na, K., Lee, E.Y., Lee, H.J., Kim, K.Y., Lee, H., Jeong, S.K., Jeong, A.S., Cho, S.Y., Kim,

S.A., Song, S.Y., 2009. Human plasma carboxylesterase 1, a novel serologic biomarker candidate for hepatocellular carcinoma. Proteomics 9, 3989-3999.

Nadaoka, I., Yasue, M., Sami, M., Kitagawa, Y., 2012. Oral administration of Cimicifuga racemosa extract affects immobilization stress-induced changes in murine cerebral monoamine metabolism. Biomedical research (Tokyo, Japan) 33, 133-137.

Niehaus, J.L., Liu, Y., Wallis, K.T., Egertova, M., Bhartur, S.G., Mukhopadhyay, S., Shi, S., He, H., Selley, D.E., Howlett, A.C., Elphick, M.R., Lewis, D.L., 2007. CB1 cannabinoid receptor activity is modulated by the cannabinoid receptor interacting protein CRIP 1a. Molecular pharmacology 72, 1557-1566.

Pannemans, D.L., van den Berg, H., Westerterp, K.R., 1994. The influence of protein intake on vitamin B-6 metabolism differs in young and elderly humans. The Journal of nutrition 124, 1207-1214.

Parra, M., Stahl, S., Hellmann, H., 2018. Vitamin B(6) and Its Role in Cell Metabolism and Physiology. Cells 7.

Peng, X.C., Gong, F.M., Chen, Y., Qiu, M., Cheng, K., Tang, J., Ge, J., Chen, N., Zeng, H., Liu, J.Y., 2016. Proteomics identification of PGAM1 as a potential therapeutic target for urothelial bladder cancer. Journal of proteomics 132, 85-92.

Prickaerts, J., Koopmans, G., Blokland, A., Scheepens, A., 2004. Learning and adult neurogenesis: Survival with or without proliferation? Neurobiology of Learning and Memory 81, 1-11.

Puig, M.V., Artigas, F., Celada, P., 2005. Modulation of the activity of pyramidal neurons in rat prefrontal cortex by raphe stimulation in vivo: involvement of serotonin and GABA. Cerebral cortex (New York, N.Y. : 1991) 15, 1-14.

Puig, M.V., Celada, P., Diaz-Mataix, L., Artigas, F., 2003. In vivo modulation of the activity of pyramidal neurons in the rat medial prefrontal cortex by 5-HT2A receptors: relationship to thalamocortical afferents. Cerebral cortex (New York, N.Y. : 1991) 13, 870-882.

Puig, M.V., Ushimaru, M., Kawaguchi, Y., 2008. Two distinct activity patterns of fast-spiking interneurons during neocortical UP states. Proceedings of the National Academy of Sciences of the United States of America 105, 8428-8433.

Riggs, K.M., Spiro, A., 3rd, Tucker, K., Rush, D., 1996. Relations of vitamin B-12, vitamin B-6, folate, and homocysteine to cognitive performance in the Normative Aging Study. The American journal of clinical nutrition 63, 306-314.

Rose, C.S., Gyorgy, P., Butler, M., Andres, R., Norris, A.H., Shock, N.W., Tobin, J., Brin, M., Spiegel, H., 1976. Age differences in vitamin B6 status of 617 men. The American journal of clinical nutrition 29, 847-853.

Rowland, N.E., Dunn, A.J., 1995. Effect of dexfenfluramine on metabolic and neurochemical measures in restraint-stressed ob/ob mice. Physiology & behavior 58, 749-754.

Sahay, A., Hen, R., 2007. Adult hippocampal neurogenesis in depression. Nature neuroscience 10, 1110-1115.

Sailor, K.A., Schinder, A.F., Lledo, P.M., 2016. Adult neurogenesis beyond the niche: its potential for driving brain plasticity. Current opinion in neurobiology 42, 111-117.

Salvi, R., Steigleder, T., Schlachetzki, J.C., Waldmann, E., Schwab, S., Winner, B., Winkler, J., Kohl, Z., 2016. Distinct Effects of Chronic Dopaminergic Stimulation on Hippocampal Neurogenesis and Striatal Doublecortin Expression in Adult Mice. Frontiers in neuroscience 10, 77.

Sanzey, M., Abdul Rahim, S.A., Oudin, A., Dirkse, A., Kaoma, T., Vallar, L., Herold-Mende, C., Bjerkvig, R., Golebiewska, A., Niclou, S.P., 2015. Comprehensive analysis of glycolytic enzymes as therapeutic targets in the treatment of glioblastoma. PloS one 10, e0123544.

Singh, C., Bortolato, M., Bali, N., Godar, S.C., Scott, A.L., Chen, K., Thompson, R.F., Shih, J.C., 2013. Cognitive abnormalities and hippocampal alterations in monoamine oxidase A and B knockout mice. Proceedings of the National Academy of Sciences 110, 12816-12821.

Spinneker, A., Sola, R., Lemmen, V., Castillo, M.J., Pietrzik, K., Gonzalez-Gross, M., 2007. Vitamin B6 status, deficiency and its consequences--an overview. Nutricion hospitalaria 22, 7-24.

Stenfors, C., Ross, S.B., 2002. Evidence for involvement of 5-hydroxytryptamine(1B)

autoreceptors in the enhancement of serotonin turnover in the mouse brain following repeated treatment with fluoxetine. Life sciences 71, 2867-2880.

Sultana, R., Boyd-Kimball, D., Cai, J., Pierce, W.M., Klein, J.B., Merchant, M., Butterfield, D.A., 2007. Proteomics analysis of the Alzheimer's disease hippocampal proteome. Journal of Alzheimer's disease : JAD 11, 153-164.

Sultana, R., Boyd-Kimball, D., Poon, H.F., Cai, J., Pierce, W.M., Klein, J.B., Merchant, M., Markesbery, W.R., Butterfield, D.A., 2006. Redox proteomics identification of oxidized proteins in Alzheimer's disease hippocampus and cerebellum: an approach to understand pathological and biochemical alterations in AD. Neurobiology of aging 27, 1564-1576.

Swanson, L.W., 1982. The projections of the ventral tegmental area and adjacent regions: a combined fluorescent retrograde tracer and immunofluorescence study in the rat. Brain research bulletin 9, 321-353.

Tipton, K.F., Boyce, S., O'Sullivan, J., Davey, G.P., Healy, J., 2004. Monoamine oxidases: certainties and uncertainties. Current medicinal chemistry 11, 1965-1982.

Uabundit, N., Wattanathorn, J., Mucimapura, S., Ingkaninan, K., 2010. Cognitive enhancement and neuroprotective effects of Bacopa monnieri in Alzheimer's disease model. Journal of ethnopharmacology 127, 26-31.

Westermeier, R., Marouga, R., 2005. Protein detection methods in proteomics research. Bioscience reports 25, 19-32.

Wilson, K.E., Marouga, R., Prime, J.E., Pashby, D.P., Orange, P.R., Crosier, S., Keith, A.B., Lathe, R., Mullins, J., Estibeiro, P., 2005. Comparative proteomic analysis using samples obtained with laser microdissection and saturation dye labelling. Proteomics 5, 3851-3858.

Xapelli, S., Agasse, F., Sarda-Arroyo, L., Bernardino, L., Santos, T., Ribeiro, F.F., Valero, J., Braganca, J., Schitine, C., de Melo Reis, R.A., Sebastiao, A.M., Malva, J.O., 2013. Activation of type 1 cannabinoid receptor (CB1R) promotes neurogenesis in murine subventricular zone cell cultures. PloS one 8, e63529.

Xu, J.Y., Chen, R., Zhang, J., Chen, C., 2010. Endocannabinoids differentially modulate synaptic plasticity in rat hippocampal CA1 pyramidal neurons. PloS one 5, e10306.

Yarlagadda, A., Clayton, A.H., 2007. Blood brain barrier: the role of pyridoxine. Psychiatry (Edgmont (Pa. : Township)) 4, 58-60.

Yoo, D.Y., Kim, W., Kim, D.W., Yoo, K.-Y., Chung, J.Y., Youn, H.Y., Yoon, Y.S., Choi, S.Y., Won, M.-H., Hwang, I.K., 2011. Pyridoxine enhances cell proliferation and neuroblast differentiation by upregulating the GABAergic system in the mouse dentate gyrus. Neurochemical research 36, 713-721.

Yoo, D.Y., Kim, W., Kim, I.H., Nam, S.M., Chung, J.Y., Choi, J.H., Yoon, Y.S., Won, M.-H., Hwang, I.K., 2012a. Combination effects of sodium butyrate and pyridoxine treatment on cell proliferation and neuroblast differentiation in the dentate gyrus of D-galactose-induced aging model mice. Neurochemical research 37, 223-231.

Yoo, D.Y., Kim, W., Yoo, K.Y., Nam, S.M., Chung, J.Y., Yoon, Y.S., Won, M.H., Hwang, I.K., 2012b. Effects of pyridoxine on a high-fat diet-induced reduction of cell proliferation and neuroblast differentiation depend on cyclic adenosine monophosphate response element binding protein in the mouse dentate gyrus. Journal of neuroscience research 90, 1615-1625.

Zhao, C., Deng, W., Gage, F.H., 2008. Mechanisms and Functional Implications of Adult Neurogenesis. Cell 132, 645-660.

국문초록

Pyridoxine으로도 잘 알려진 비타민B_6는 효소활성을 돕는 보조인자로서 160개가 넘는 생화학적 반응에 관여한다. Pyridoxal 5'-phosphate (PLP)는 비타민B_6의 활성화 형태로써 세로토닌, 도파민, 노르에피네프린, GABA를 포함한 신경전달물질을 합성하는데 작용한다. 비타민B_6의 결핍은 뇌에서 기억과 인지의 기능에 영향을 줄 수 있으며 파킨슨병, 알츠하이머병, 우울증 같은 신경학적 질병과 연관될 수 있음이 알려져 있다. 본 연구의 목적은 pyridoxine의 투여가 마우스의 해마에서 기능적으로 어떠한 영향을 끼치는지 확인하고, 더 나아가 단백체 분석을 통해 해마의 신경세포재생을 조절하는 물질을 찾아내어 그 기전을 밝히는데 있다.

본 실험에서는 8주령의 C57BL/6J 마우스를 대상으로 생리식염수 (vehicle) 또는 350mg/kg pyridoxine hydrochloride를 3주간 하루 2회씩 복강투여하였다. 투여 20일과 21일째에 새로운 개체 인식 테스트 (novel object recognition test)를 수행하였으며 그 후 동물을 희생하여 면역조직화학적염색, 고성능 액체 크로마토그래피 (HPLC; high-performance liquid chromatography)분석을 통해 해마의 기억 능력 및 신경세포재생에 미치는 변화를 확인하였다. pyridoxine의 투여는 새로운 개체 인식 테스트에 기초한 discrimination index를 유의적으로 증가시켰으며 세로토닌 (5-HT)과 타이로신 수산화효소 (tyrosine hydroxylase) 또한 유의적으로 증가시킴을 확인할 수 있었다. 또한 신경세포재생을 촉진시키는 것이 확인된 pyridoxine의 투여가 마우스의 해마에서 어떤 단백질을 변화시키는지 알아보기 위하여 2차원 전기영동 (2D-DIGE)과 말디토프 질량분석기를 사용하여 단백체 분석을 실시하였다. 그 결과 pyridoxine 투여군에서 1.5배 이상 증가한 단백질은 PGAM1, 1.5배 이상 감소한 단백질은 CRIP1으로 확인되었다. 이 결과는 western blot 분석과 정량적 실시간 중합효소

연쇄반응(quantitative real time polymerase chain reaction) 분석, 면역조직화학적염색을 통해 입증하였다.

CRIP1a siRNA의 투여는 해마에서 세포 증식 및 신경모세포 분화 뿐만 아니라 discrimination index를 유의적으로 증가시켰다. 게다가 CB1 cannabinoid 수용체의 길항제인 rimonabant의 투여는 해마의 치아이랑에서 새로운 개체 인식 기억, 타이로신 수산화효소의 면역반응성, 그리고 세포 증식 및 신경모세포 분화를 유의적으로 감소시켰다.

또한 해마의 치아이랑에서 PGAM1의 효과를 알아보기 위해 혈액-뇌 장벽 (blood-brain barrier)을 통과할 수 있도록 Tat-PGAM1 융합 단백질을 제조하여 8주령의 C57BL/6J 마우스에 3주간 투여하였다. Western blot 분석 결과, 대조군, Tat-펩타이드 투여군, 대조-PGAM1 투여군에 비하여 Tat-PGAM1 투여군의 해마조직에서 PGAM1 단백질 발현량이 유의적으로 증가함을 확인하였다. Tat-PGAM1의 투여는 해마의 치아이랑에서의 세포 증식 및 신경모세포 분화 그리고 discrimination index를 유의적으로 증가시킨 반면 대조-PGAM1 투여는 유의적 변화를 보이지 않았다.

위 실험 결과들을 통해 비타민B_6의 투여가 세로토닌의 turnover와 타이로신 수산화효소의 면역반응성을 증가시키면서 해마의 기능을 촉진한다는 것을 확인하였다. 또한 단백체 분석을 통하여 선별된 단백질인 CRIP1a와 PGAM1에 대하여 해마의 신경세포재생에서의 효과를 확인한 결과, pyridoxine의 투여가 가져온 긍정적 변화는 CRIP1a와 CB1R signaling의 조절 그리고 CREB의 인산화를 통한 PGAM1의 up-regulation에 기인한 것으로 추측된다.

주요어 : 비타민B_6, 해마, 신경세포재생, CB1 cannabinoid receptor-interacting protein 1, phosphoglycerate mutase 1, C57BL/6 마우스
학번 : 2012-21550